Machine Learning-Based Power Estimation and Coastal Adaptation of Wave Energy Converters

A thesis proposal presented to the faculty of the Graduate School of Western Carolina University in partial fulfillment of the requirements for the degree of Master of Science in Engineering Technology

By
Omer Mert Gursel

Director: Dr. Bora Karayaka
Professor
School of Engineering + Technology

Committee Members:
Dr. Paul Yanik, School of Engineering + Technology
Dr. Tarek Kandil, School of Engineering + Technology

April 2025

ACKNOWLEDGEMENTS

I am very honored to be a part of Western Carolina University. The great support and guidance of the faculty members have been instrumental in my academic and personal development, enriching my knowledge and fueling my passion for learning.

I am especially grateful to Dr. Bora Karayaka for his extraordinary guidance throughout my research. His introduction to the field of wave energy converters and machine learning has opened new and exciting avenues in my academic journey. It has been a privilege to work under his guidance; his dedication and thoroughness to research has continuously motivated me to achieve excellence. I am truly fortunate to have him as my thesis advisor.

I would also like to extend my heartfelt thanks to my committee members, Dr. Paul Yanik and Dr. Tarek Kandil, for their insightful feedback and valuable contributions to my work. Their support and expertise have greatly enhanced the quality of this research.

To my fellow graduate students, I would like to thank you for your cooperation, encouragement, and friendship throughout this journey.

Finally, I am deeply grateful to my family for their love, patience, and support. Their belief in me has been the foundation of my success.

LIST OF TABLES

LIST OF FIGURES

ABSTRACT

Machine Learning-Based Power Estimation and Coastal Adaptation of Wave Energy Converters

Omer Mert Gursel, MSET

Western Carolina University (April 2025)

Director: Dr. Bora Karayaka

This thesis presents an integrated approach to estimating and optimizing the power output of a Wave Energy Converter (WEC) using machine learning, followed by its adaptation to the wave characteristics of the North Carolina coast. Initially, a neural network model was developed to estimate a custom designed WEC's power output based on wave height, wave period, and resonance conditions, defined by the phase alignment between the wave excitation force and the power take-off (PTO) system. A simulation-generated dataset was used to train and validate the model, achieving a maximum prediction error below 1% on randomly generated test data. A heatmap was generated to determine the optimal neural network topology, minimizing errors across various configurations. The trained model was applied to develop a Maximum Power Point Tracking (MPPT) strategy, confirming its reliability and practical application in real-time control scenarios. To enhance real-world applicability, the machine learning-based estimation framework was extended and integrated into a comprehensive wave resource assessment tailored for the North Carolina coastline. Historical wave data from July 2005 to December 2018, obtained through WaveWatch III and HYCOM models, were used to analyze 491 offshore locations. Sea states were segmented in three-hour intervals to capture statistical wave behavior, seasonal variability, and energy flux patterns. A Joint Probability Distribution (JPD) of significant wave height and peak wave period was constructed to guide the design and sizing of the Department of Energy's

Reference Model 3 (RM3) WEC, ensuring that it operates efficiently under the region's most frequent wave conditions. A MATLAB/Simulink-based WEC model was developed in WEC-Sim design tool using a two-body point absorber and a slider-crank mechanism to convert heave motion into rotational mechanical power. A reactive control strategy was applied to synchronize the float's motion with the incoming wave force, thereby maximizing power extraction. Site selection for deployment was based on mechanical power outputs across different WEC scales (full, half, and one-third), resulting in the identification of 12 optimal locations. Additionally, the impact of various array configurations was analyzed to determine the most cost-effective deployment strategies in terms of Levelized Cost of Energy (LCOE).To support MPPT development for this new WEC, a detailed dataset covering 432 unique sea state scenarios was constructed, varying significant wave heights (0.75–4.75 m), peak wave periods (3.5–12.5 s), and eight time shift values (−0.25 to 0.35 s) representing the timing offset between wave force and float velocity. Analysis showed that while in-phase alignment (0 s) yielded optimal output in certain scenarios, slight negative time shifts (−0.05 s, −0.15 s and -0.25 s) resulted in higher power capture in higher sea states, emphasizing the importance of dynamic phase adjustment. These findings demonstrate the potential of machine learning to enhance wave energy system performance and support the design of adaptive, cost-efficient WECs tailored to the wave spectrum of the U.S. East Coast.

CHAPTER 1: INTRODUCTION AND LITERATURE REVIEW

Global energy demand continues to increase steadily due to population growth [1] and growing demand from other loads such as AI servers. Traditional energy sources, especially fossil fuels, are finite and cause significant environmental pollution, leading to global warming, air quality deterioration, and ecological degradation [2]. In contrast, renewable energy offers a sustainable and environmentally friendly alternative. These systems are increasingly being used to power residential areas, industrial operations, and transportation in many regions, minimizing environmental damage [3].

Renewable energy sources are virtually limitless, making them indispensable for meeting long-term energy needs [5]. They use natural resources such as sunlight, wind, sea or ocean waves, and geothermal heat, which are constantly replenished in a natural balance. While fossil fuels are still effective for energy production today, their inevitable depletion necessitates transitioning to sustainable alternatives to ensure energy security. This transition is critical not only for energy requirements but also for reducing the environmental impact caused by fossil fuel consumption, including greenhouse gas emissions, oil spills, and habitat destruction [5–6].

Wave energy is a clean and renewable resource generated through wave energy converters that capture ocean surface waves' kinetic and potential energy [7]. However, its adoption remains limited due to several challenges, including high costs, infrastructure, regulatory challenges, and possible environmental effects [8]. With the rising demand for sustainable energy solutions, interest and investment in wave energy research are steadily increasing. Ocean wave energy, one of the most promising renewable energies, offers a strong and largely untapped potential [8]. Despite the untapped potential of wave energy, technical difficulties in converting sea waves into electricity hinder its adoption and diffusion [9].

The variable nature of ocean waves offers a robust and reliable energy estimation approach addressed through machine learning techniques. In this thesis, a machine learning algorithm is employed and demonstrated to estimate ocean wave variability and power output of a wave energy converter to achieve this potential. This study explores the architecture of an artificial neural network, focusing on applying machine learning methods to improve the precision and effectiveness of power output estimations for Maximum Power Point Tracking (MPPT). Previous studies have shown that when the neural network is trained with sufficient data, neural networks can determine relationships between past and future wave strengths [10]. However, due to the nature of waves, existing studies need to be improved to directly predict the power output of Wave Energy Converters (WECs) [11].

Wave Energy Converters (WECs) are designed to convert ocean waves into electrical energy. Maximum Power Point Tracking (MPPT) methods were developed to maximize the efficiency of these systems, primarily due to the highly variable and unpredictable nature of wave energy. MPPT algorithms are required to optimize the power output of WEC systems by continuously adjusting system parameters to operate at their most efficient level. Traditional MPPT methods often fall short when dealing with the complex and dynamic environment of ocean waves and the limitations associated with Power Take-Off Unit (PTO) systems.

In this thesis, machine learning is used to develop a data-driven Maximum Power Point Tracking (MPPT) method for a Wave Energy Converter–Power Take-Off (WEC-PTO) system, enhancing real-time performance by accurately modeling the system's complex dynamics with an extensive training dataset. Integrating machine learning into the MPPT control strategy allows for a more adaptive and responsive system capable of adjusting to the highly variable nature of ocean waves. The proposed method is trained on power output data calculated under real-world

conditions and is validated using irregular wave scenarios. This comprehensive approach aims to advance renewable energy technologies by demonstrating the potential of machine learning to improve the efficiency and reliability of wave energy conversion systems.

The machine learning method for MPPT summarized above is based on a hypothetical WEC and sea states. To apply this method to a more realistic WEC and sea states, this thesis also investigates applicability of this approach to a real WEC adapted for North Carolina coastal conditions while trying to minimize its cost.

There is a significant lack of Wave Energy Converter (WEC) systems specifically adapted to the wave conditions along the North Carolina coastline. Much of the existing technology is proprietary, which restricts access to design details and limits opportunities for customization. This study modifies the Reference Model 3 (RM3), a point absorber WEC originally developed by the U.S. Department of Energy's National Renewable Energy Laboratory, as detailed by Neary et al. (2014). Although the RM3 was initially intended for deep-water deployment off the coast of California, it serves as a suitable baseline model for adaptation to different environments.

Following this phase, the Balanced Cost of Energy (LCOE) was examined to assess the economic viability of WEC deployment off the coast of North Carolina. Initial studies focused on the benchmark RM3-WEC heaving buoy design, providing insight into its energy conversion efficiency and cost metrics. To expand the analysis, we compared the heaving buoy design of the RM3-WEC with a slider-crank WEC design. The comparison focused on evaluating the Levelized Cost of Energy (LCOE) for each configuration based on specific site conditions, array layouts, WEC scaling factors, and power output limitations.

The present work focuses on scaling and adapting the RM3 system for deployment in the relatively shallow waters of North Carolina's offshore environment. Full scale, half scale and one-

third-scale version of the RM3 was developed to match the wave characteristics and site-specific conditions along the state's coastline. Special attention was given to optimizing the Power Take-Off (PTO) system and mooring configurations to achieve resonant coupling with prevailing wave frequencies, thereby maximizing mechanical energy capture.

In summary, this research contributes to advancing wave energy technologies in the southeastern United States by integrating machine learning-enhanced control strategies with cost-optimized and site-adapted WEC designs. By combining technical modeling, economic assessment, and site-specific adaptation, the study demonstrates a scalable approach to integrating wave energy into North Carolina's renewable energy portfolio, paving the way for more resilient and diversified marine energy systems.

CHAPTER 2: METHODOLOGY

2.1 Integration of Machine Learning for Enhanced Wave Energy Converter Power Output Estimation

2.1.1 Overall System Model

This thesis explores a wave energy converter (WEC) system incorporating a slider-crank mechanism as its power take-off system (PTOS). This setup represents a form of linear to rotary PTOS, making it well-suited for large-scale energy harvesting applications. The study evaluates the system's performance under regular and irregular wave conditions, aiming to reflect realistic ocean environments. A rule-based control strategy improves the system's adaptability [13]. The structure of the slider-crank WEC used in this analysis is shown in Figure 2.1.

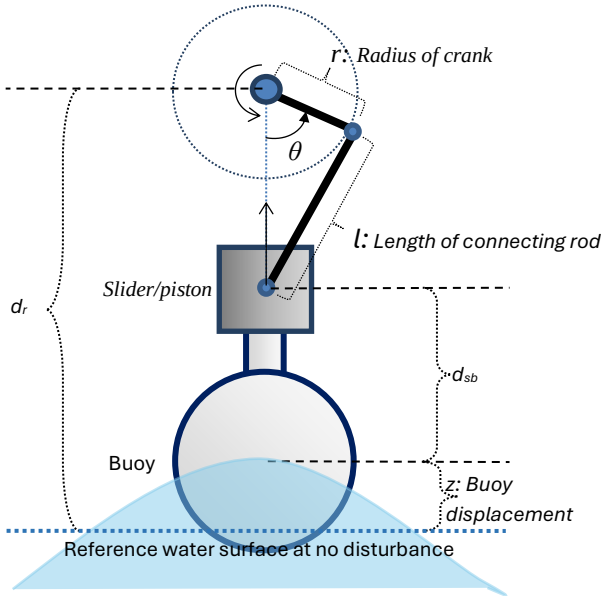

Figure 2.1: Slider crank WEC structure [12]

The wave energy converter's (WEC) hydrodynamic model is based on a semi-submerged spherical buoy with a radius of 5 meters and focusing on its vertical (heave) motion. The interaction between the buoy and the wave-induced forces is calculated by the Cummins equation, which expresses the hydrodynamic forces resulting from the buoy's motion as expressed in

Equation (1). A key aspect of this model is the radiation force, which is estimated to be using analytical methods tailored to the buoy's shape. This leads to the formulation of a transfer function that connects the buoy's velocity to the corresponding radiation force.

$$(M + a_{\infty})\ddot{z}(t) + \int_{-\infty}^{t} H_{rad}(t-\tau)\,\dot{z}(\tau)d\tau + S_b z(t) = F_e(t) - F_u(t) \quad (1)$$

To simulate irregular wave conditions, this study utilizes the Joint North Sea Wave Project (JONSWAP) spectrum, which includes peak enhancement factor (γ). This spectral model provides a more realistic representation of sea states than simpler models by accounting for the energy distribution across frequencies and the growth phase of wind-generated waves. The irregular wave profile is constructed by summing multiple sinusoidal wave components, each with unique amplitudes, angular frequencies, and phase shifts. In this approach, angular frequencies span from 0.5 to 1.4 radians per second, increasing in steps of 0.01 radians per second. The amplitudes of these wave components are calculated based on the JONSWAP spectrum. Wave component amplitudes initial phases are randomly assigned values between 0 and 2π, which can be expressed in Equation (2) [12–13].

$$S(f) = \frac{\alpha_j g^2}{(2\pi)^4} f^{-5} exp\left[-\frac{5}{4}\left(\frac{f_p}{f}\right)^4\right] \gamma^{\Gamma} \quad (2)$$

In this context, α_j is a function of wind speed and fetch length, f_p represents the peak frequency of the irregular wave spectrum, f refers to wave component frequencies, and γ^{Γ} denotes the peak enhancement factor and Γ expressed as follows:

$$\Gamma = exp\left[\frac{\left(\frac{f}{f_p}\right)^2}{\sqrt{2}\,\sigma}\right], \sigma = \begin{cases} 0.07 & f \le f_p \\ 0.09 & f > f_p \end{cases} \quad (3)$$

2.1.2 Machine Learning Based Model

This thesis introduces a machine learning-based Maximum Power Point Tracking (MPPT) approach tailored for a Wave Energy Converter with a Power Take-Off (WEC-PTO) system. The control strategy is centered around the concept of *Time Shift*, which quantifies the resonance condition and serves as the primary control variable for optimizing power extraction. A time shift of zero indicates that the wave excitation force and the buoy's velocity are perfectly aligned—in other words, they are in-phase—resulting in suboptimal energy capture. A negative time shift suggests the buoy's velocity lags behind the excitation force, whereas a positive shift means it leads.

Figure 2.2 presents a block diagram of the complete WEC-PTO control architecture, including the electric drive system. The section labeled "ANN Model for MPPT" in the lower left corner is expanded in detail in Figure 2.3. The objective is to leverage an artificial neural network (ANN), a machine learning tool, to predict power output across various wave conditions. The ANN uses wave height, wave period, and time shift as input parameters to estimate the WEC's power output. These estimated outputs are then passed to the "Best Resonance Condition Search" block, which employs a binary search algorithm to iteratively identify the optimal time shift for the shaft angle controller to achieve Maximum Power Point Tracking (MPPT). Finally, the highest estimated power output is matched with its corresponding time shift, determining the optimal operating condition.

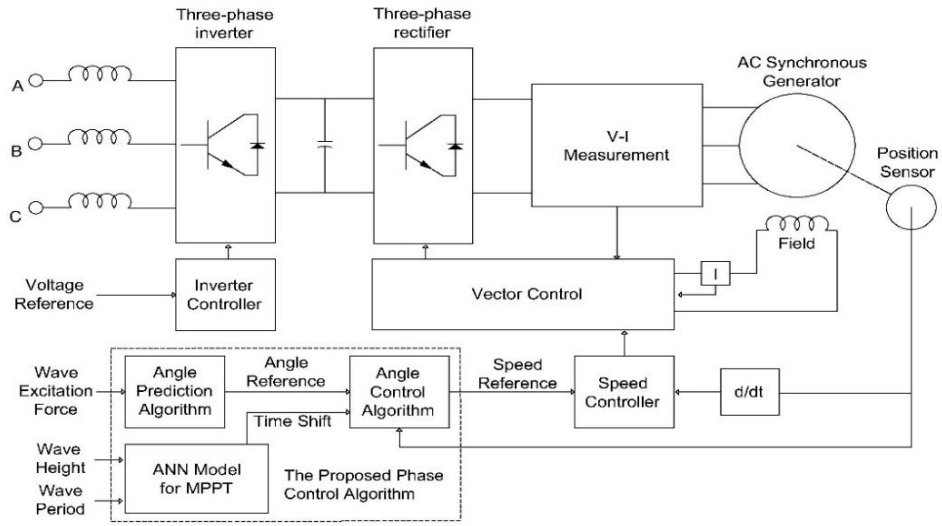

Figure 2.2: WEC-PTO control schematics of the machine drive system [17].

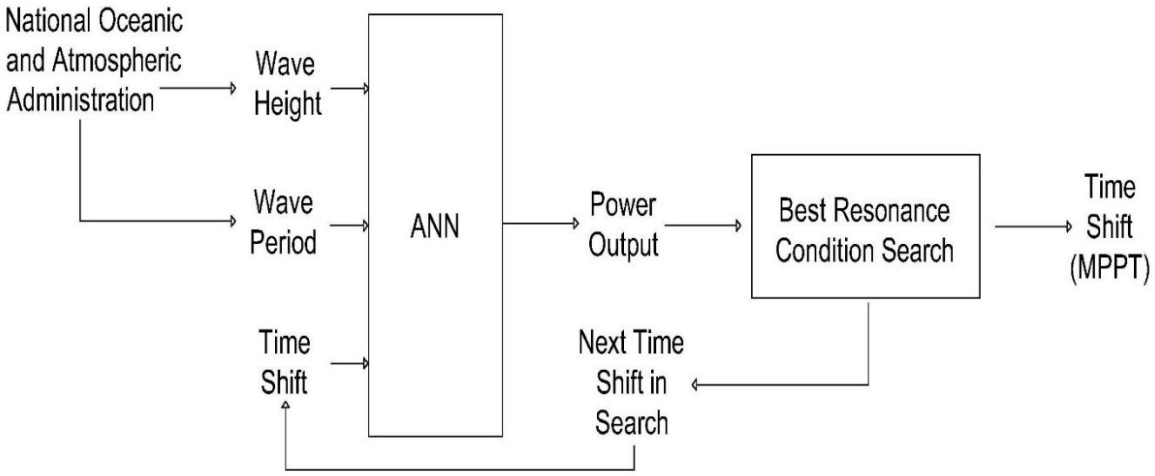

Figure 2.3: ANN model for MPPT [17].

The methodology involves evaluating power output under both regular and irregular waves. Training datasets are constructed with uniformly spaced values of wave height, period, and time shift, while test datasets are selected from within the same range to validate performance. The structure and intervals of these datasets are outlined in Table 2.1 (regular waves) and Table 2.2 (irregular waves), each highlighting specific combinations of wave parameters and time shifts.

Table 2.1: Regular Waves Data Set Distribution [17].

Dataset	**Wave Heights - H (m)**	**Wave Periods - T (s)**	**Time Shifts (s)**	**Outputs**
Training	1.00, 1.25, 1.50, 1.75, 2.00	6 to 10 seconds (11 intervals)	-1 to 1 (11 intervals)	Actual power outputs
Test	1, 1.333, 1.667, 2	6, 7, 8, 9, 10	-1 to 1 (0.1 s step size)	Actual power outputs

Table 2.2: Irregular Waves Data Set Distribution [17].

Dataset	**Significant Wave Heights - H_{m0} (m)**	**Peak Periods - T_p (s)**	**Time Shifts (s)**	**Outputs**
Training	1.1314 to 3 (11 intervals)	6 to 12 (11 intervals)	-1 to 1 (11 intervals)	Actual power outputs
Test	1.1314, 1.4142, 1.6971, 1.9799, 2.2627, 2.5456, 3	6, 7, 8, 9, 10, 11, 12	-1 to 1 (0.1 s step size)	Actual power outputs

Several artificial neural network (ANN) configurations were evaluated to estimate the accurate power outputs. Three different architectures were tested. The first used a single hidden layer with 10 neurons. The second also had a single hidden layer with 20 neurons. The third architecture included two hidden layers with 10 neurons in each layer. Various data partitioning schemes for training, validation, and testing were explored to identify the most effective setup. A fixed 70% of the dataset was used for training, while the validation portion varied from 0% to 30%, with the remainder allocated for testing. The validation dataset was used to implement early

stopping in MATLAB™, a technique that stops the training process once the validation performance shows no further improvement [15].

The procedure started by generating datasets that included input parameters—wave height, wave period, and time shift—along with their corresponding power outputs obtained from WEC simulations. These datasets were then used to develop and train neural networks using selected hidden layer configurations. The training process was carried out using the Levenberg–Marquardt backpropagation algorithm (trainlm) [16].

The sigmoid function is a mathematical operation that maps input values to a range between 0 and 1, defined in Equation (3). It is widely used in neural networks as an activation function to introduce non-linearity, which is essential for learning complex and nonlinear patterns within data. Alongside other common activation functions such as hyperbolic tangent (tanh) and Rectified Linear Unit (ReLU), sigmoid enables the network to detect intricate relationships. In this study, the sigmoid function was selected due to its effectiveness in minimizing estimation errors and improving overall model accuracy [13]. After determining the activation function, the dataset was divided into training, validation, and testing sets based on specified ratios.

$$f(x) = \frac{1}{1 + e^{-x}} \tag{4}$$

Each ANN configuration was trained, validated, and tested across 100 independent runs to ensure consistent and reliable results. After each training session, the resulting network was saved for future use. The performance of the trained models was evaluated by calculating the absolute error between the predicted and actual power outputs. The error rates from each run were calculated and recorded, as shown in Equation (4).

$$E_r = \left| \frac{Actual\ Power\ Output - Estimated\ Power\ Output}{Actual\ Power\ Output} \right| \times 100 \tag{5}$$

The outcomes of the analysis are visualized through a heatmap, which highlights the average error rates across various combinations of hidden layer sizes and validation ratios. Additionally, 2D surface plots are generated to illustrate how these parameters interact and influence estimation error.

The artificial neural network (ANN) models are tested using randomly generated datasets under both regular and irregular wave conditions as documented in Appendix A. The configuration yielding the lowest error is selected and examined to assess its accuracy in predicting power output.

This research conducted a structured evaluation of multiple neural network architectures to establish a reliable MPPT strategy for the WEC-PTO system. By incorporating machine learning—specifically ANNs—the study achieved enhanced accuracy and efficiency in estimating power output under dynamic wave scenarios, outperforming traditional approaches.

A binary search algorithm is used to determine the phase shift that yields the maximum power output as indicated in Appendix B. This method iteratively refines the optimal time shift for different sea states, defined by specific combinations of wave height and period. The process involves comparing power output predictions from the most accurate neural network with corresponding simulation results. By repeatedly narrowing the search interval and concentrating on the range producing higher power output, the algorithm identifies the best time shift to maximize energy capture under varying ocean conditions.

2.2 Levelized Cost of Energy (LCOE) Analysis for Wave Energy Converters (WECs)

2.2.1 Wave Energy Converter Model

This phase of the study focuses on evaluating the power generation capability of the proposed the Department of Energy's Reference Model 3 (RM3) Wave Energy Converter (WEC) model, developed using MATLAB/Simulink (MathWorks, Natick, MA, USA) [18]. The model

comprises two main subsystems: a two-body point absorbed system based on the WEC-Sim Reference Model 3 (RM3), integrated with a slider-crank linkage mechanism, and a power take-off (PTO) system that includes a gearbox, generator, power electronics converter, and associated control components.

The slider is mechanically connected to the float of the RM3 structure. The crank linkage, which pivots within the slider, converts the float's vertical heave motion into unidirectional rotational motion. This rotation drives the rotary electrical machine, managed by its control system. The crankshaft, attached to the spar, rotates freely and transmits torque to the generator through the gearbox.

The key system variables illustrated in Figure 2.4 are as follows:

- T_m: Slider-crank drive torque (WEC-PTO torque)
- F_b : Force exerted by the float
- r: Crankshaft radius
- l: Length of the connecting arm
- θ: Crankshaft angle

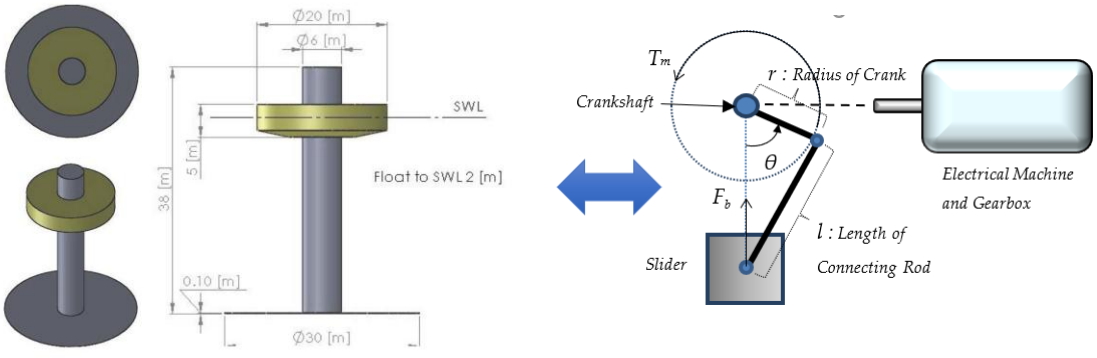

(**a**) (**b**)

Figure 2.4: Integration of various components of the WEC system. (**a**) WEC-Sim RM3, (**b**) slider-crank linkage model, rotary electrical machine, and gearbox [20].

The electrical machine generates an electromechanical torque T_m that continuously tracks the WEC-PTO torque T_m, to enable efficient energy conversion. This is achieved by controlling the machine's terminal voltage V_a , thereby regulating power flow and maximizing the average power output. The system operates under a reactive control mechanism, where energy temporarily flows both into and out of the machine to maintain unidirectional rotation [18].

The control system, shown in Figure 2.5, includes:

- F_b: Wave excitation force
- n: Shaft rotational speed
- I_a: Armature current, proportional to T_e
- Superscript (*): Reference values

In future phases of this research, the "Phase Tracking and Correction Process" blocks within the control system will be expanded to implement a Maximum Power Point Tracking (MPPT) algorithm. Currently, these blocks synchronize the excitation force and crankshaft velocity to increase power extraction ability under reactive control. A block diagram of the control system for the slider-crank-based WEC is presented in Figure 2.5.

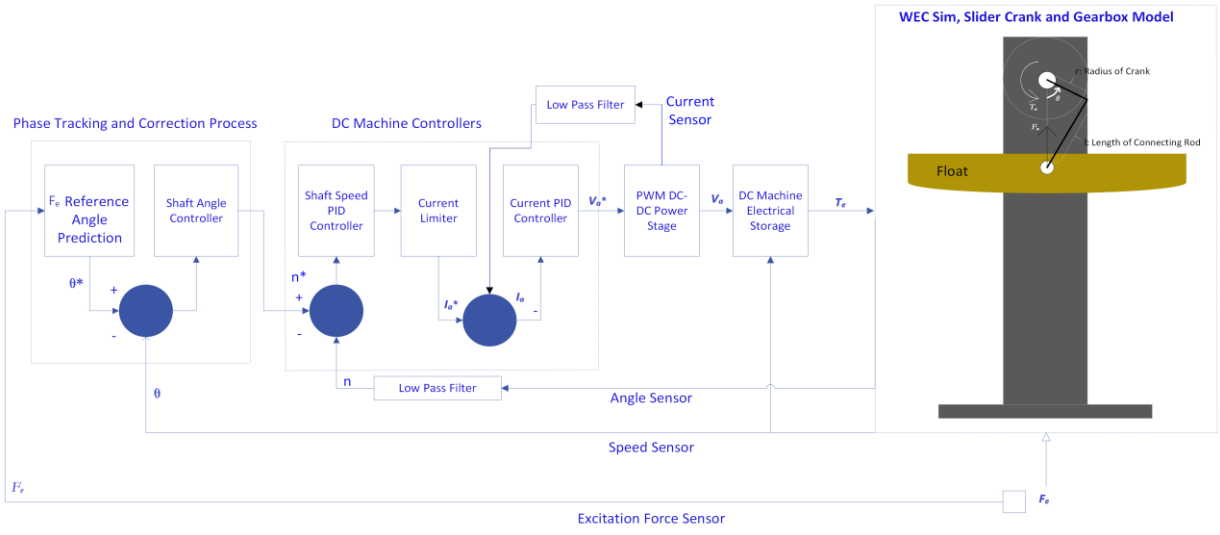

Figure 2.5: Slider crank WEC control system block diagram.

Wave Energy Converter–Power Take-Off (WEC-PTO) system was modeled as a lossless system. To conduct a comparative evaluation of the theoretical power output at each site for the RM3 WEC, two distinct configurations were considered as illustrated in Figure 2.6. The first configuration involved a fixed spar anchored to the ocean floor, while the second modeled the system as a floating structure with mooring lines in the spar. These two approaches allowed for a comprehensive assessment of how different mooring strategies affect power generation potential across various sea sites.

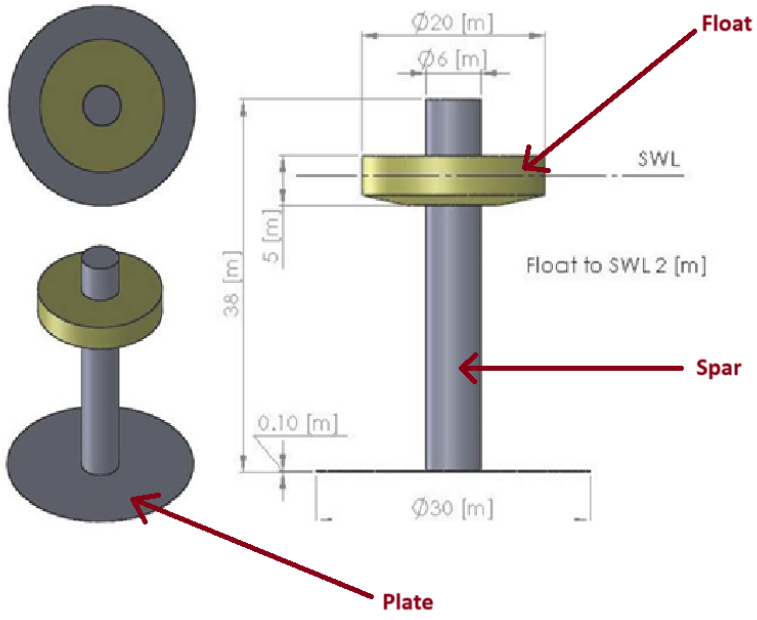

Figure 2.6: RM3 WEC Components

The second model utilized a mooring configuration, allowing the spar to move in 3 degrees of freedom. To limit this motion, mooring lines were applied in surge and heave directions. Each of these mooring lines are configured as spring elements with a stiffness coefficient of 22,500-kN for the full-scale model. The mooring lines are attached to the center of gravity location on the

spar, which is 10 m below the mean water surface. The WEC-Sim Simscape Multibody configuration of this model can be seen in Figure 2.7.

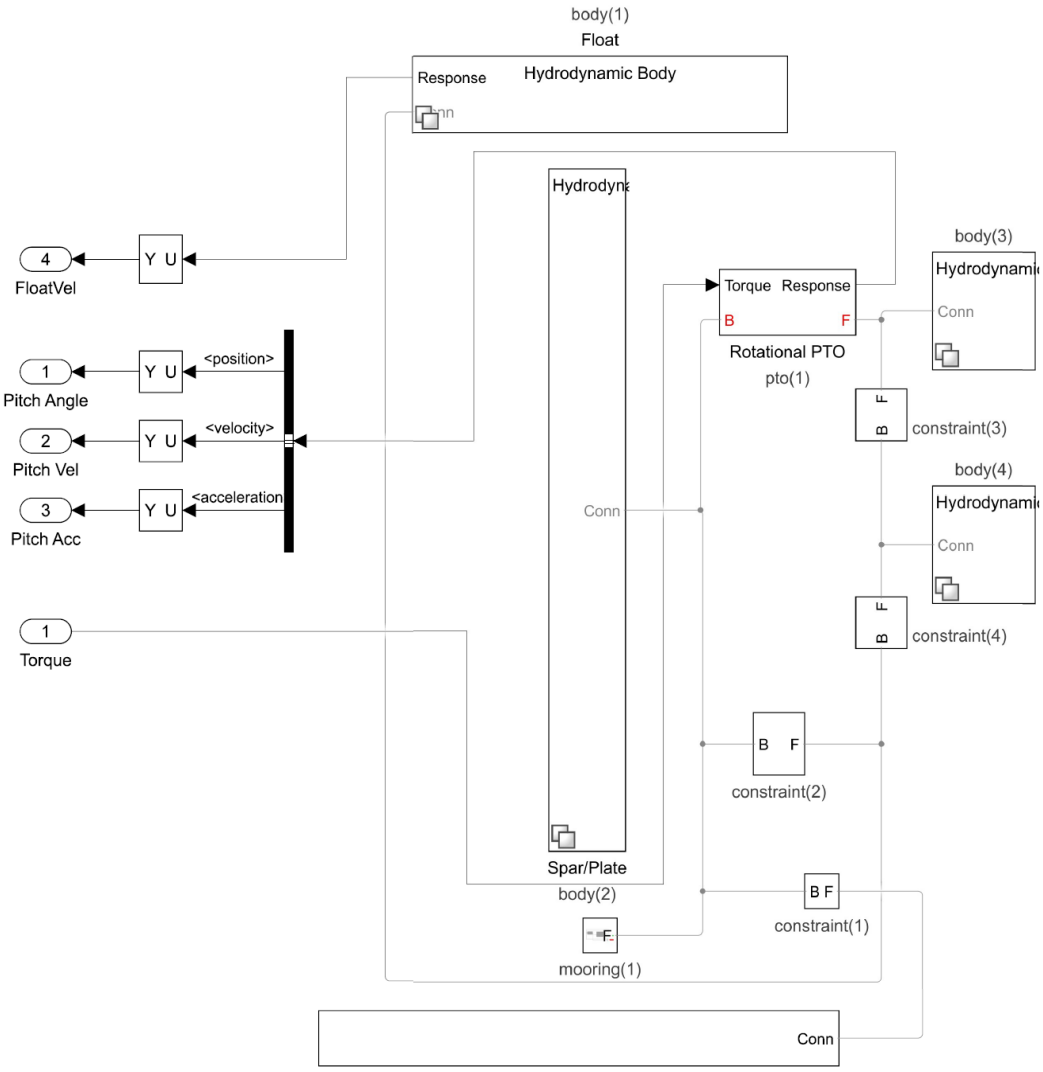

Figure 2.7: WEC-Sim mooring configuration and data acquisition in RM3 WEC.

Figure 2.7 illustrates the key components and connections within the RM3 Wave Energy Converter (WEC) model, with a focus on its mooring system and mechanical dynamics. Each element plays a critical role in the overall energy conversion process. The WEC consists of multiple bodies that function together to harness wave energy. The first body, body (1), is the float

positioned at the top of the structure. It moves in response to ocean waves and captures wave energy, transmitting this motion to the slider crank mechanism. The second body, body (2), is the spar or plate that serves as a stationary or semi-fixed base. In the floating configuration, it is stabilized by mooring lines while supporting the crankshaft and connecting arm. The third body, body (3), is the crank section of the slider crank mechanism, which rotates to convert the float's vertical heave motion into rotational motion. This motion is then transmitted through body (4), the connecting arm, which links the crank to the float and ensures smooth transfer of mechanical energy.

The Power Take-Off (PTO) system is represented by pto(1), the rotational PTO joint connected to the generator. It converts the rotational motion from the crank into electrical energy.

Several constraints are incorporated to define the mechanical interactions among components. Constraint(1) is a three degrees of freedom joint that connects the spar to the global reference frame, allowing controlled heave, surge, and pitch motions essential for floating configurations. Constraint(2) is a translational joint that connects the spar and the float, enabling relative vertical (heave) motion between the two bodies. Constraint(3) is a rotational joint that links the crank to the connecting arm, ensuring unrestricted rotation while maintaining their connection. Constraint(4) connects the connecting arm to the spar, offering the flexibility needed for efficient energy transmission from the float through the crank.

The mooring system, labeled mooring(1), consists of mooring lines that anchor the spar to the ocean floor. These lines apply restoring forces proportional to the spar's displacement, allowing limited heave, surge, and pitch movements. This stabilization mechanism ensures that the floating spar maintains its position while still allowing enough motion to facilitate continuous and efficient energy capture.

2.2.2 Site Selection and Mechanical Power Analysis

Under real sea conditions, the top 12 optimal sea sites were selected from a total of 491 sea site locations to evaluate the performance of the wave energy converter. These sites were identified based on the highest weighted average mechanical power outputs, considering the effects of mooring. While each individual scale considered ten selected sites, variations in scaling led to a total of twelve unique site locations across all scale configurations. These sites represent the most suitable geographical regions for efficient wave energy conversion.

A MATLAB script, provided in Appendix F, is generated and it allows the user to input wave height, period, and time shift values, automatically updates the corresponding parameters, runs the WEC-Sim simulation, and calculates both mechanical and electrical average power outputs.

The mechanical power outputs were further analyzed with consideration of mooring forces to provide a realistic estimation of power generation. The top-performing sites among the 491 sites, including mooring effects, are summarized in Table 2.4. A detailed comparison of mechanical power outputs across the top 7 sea sites for different scale configurations is presented in Table 2.3.

Table 2.3: Mechanical Power Outputs with Mooring for the Top 7 Sea Sites Across Different Scales

Latitude/ Longitude	1/1 Scale Power Output-Mooring (kW)	1/2 Scale Power Output-Mooring (kW)	1/3 Scale Power Output-Mooring (kW)	Capture Width Ratio (1x1 / 1x2 / 1x3)
35.3/-75.0	1,249.5	482.0	184.5	0.57 / 0.44 / 0.25
35.6/-74.8	1,243.3	478.2	183.0	0.57 / 0.44 / 0.25
35.2/-75.1	1,240.8	479.5	183.8	0.57 / 0.44 / 0.25
35.0/-75.3	1,239.1	472.8	181.4	0.57 / 0.44 / 0.25
35.1/-75.2	1,236.3	476.3	182.6	0.57 / 0.44 / 0.25
35.1/-75.1	1,233.0	477.5	183.2	0.57 / 0.44 / 0.25
35.5/-74.9	1,216.7	469.9	181.2	0.57 / 0.44 / 0.25

Table 2.4: Top 12 Optimal Sites Across All Scales.

Latitude/Longitude	Site Number	Full Scale	Half Scale	1 by 3 Scale
35.3/-75.0	164	✓	✓	✓
35.6/-74.8	127	✓	✓	✓
35.2/-75.1	169	✓	✓	✓
35.0/-75.3	157	✓	✓	✓
35.1/-75.2	186	✓	✓	✓
35.1/-75.1	180	✓	✓	✓
35.5/-74.9	174	✓	✓	✓
34.5/-74.9	142	✓	✓	✓
34.6/-75.6	220	✓	X	X
34.5/-75.7	235	✓	X	X
35.4/-74.9	150	X	✓	✓
35.5/-74.9	135	X	✓	✓

2.2.3 Power Output Matrices and Joint Probability Distributions

Power output matrices were developed for each of the three system scales to quantify the power generation capabilities of the wave energy system. These matrices were calculated across a comprehensive range of sea states, defined by significant wave heights ranging from 0.25 meters to 9.75 meters, with 0.5-meter increments, and wave energy periods ranging from 0.43 seconds to 17.67 seconds, covering a total of twenty-one energy period values.

In the analysis of the Joint Probability Distribution (JPD) of wave conditions, probability values below 0.10% were omitted to reduce data irregularities and focus the analysis on the most probable and impactful sea states. The JPD used in the site analysis is shown in Table 2.5 for a representative location at 35.6°N, 74.8°W.

Table 2.5: Joint Probability Distribution (JPD) at Site 35.6°N, 74.8°W

Hs/Te	3.88	4.74	5.6	6.47	7.33	8.19	9.05	9.91
0.25	0.041	0.058	0.028	0.099	0.206	0.165	0.094	0.044
0.75	1.354	2.812	2.297	2.16	4.996	3.53	1.546	0.682
1.25	4.463	5.712	6.072	4.014	4.741	3.75	1.901	0.988
1.75	0.85	5.109	4.49	3.222	2.399	1.92	1.497	0.762
2.25	0.039	1.238	3.546	2.633	1.714	0.913	0.713	0.41
2.75	0	0.14	1.406	1.722	1.249	0.795	0.454	0.242
3.25	0	0.019	0.245	0.773	0.704	0.608	0.283	0.173
3.75	0	0	0	0.237	0.366	0.294	0.193	0.132
4.25	0	0	0	0.03	0.162	0.193	0.171	0.052

2.2.4 Full-Scale Electrical Power Ratings and Power Output Limitations

As shown in Figure 2.5, the slider crank Wave Energy Converter (WEC) system captures wave energy through the vertical motion of a float. This float rises and falls with the heave motion of ocean waves and is mechanically connected to a crankshaft via a connecting rod. The up-and-down motion of the float is transferred through the rod, converting linear displacement into rotational motion using the slider crank mechanism. This rotational motion drives a generator through a gearbox and power electronics converter, completing the mechanical-to-electrical energy conversion process.

The maximum electrical power output recorded from this system was 1,094.58 kW. To study performance under different design limitations, three output thresholds—858 kW, 572 kW, and 286 kW—were applied to the full-scale power matrix. In each case, power values exceeding the cap were reduced to the threshold level, while values below the cap remained unchanged. This capping strategy enabled a detailed analysis of how design constraints might influence total energy production. Table 2.6 shows the full-scale power output matrix without any limitations, while Table 2.7 presents the same matrix after applying the 858-kW cap.

Table 2.6: Full Scale Power Output Matrix

Hs/Te	6.47	7.33	8.19	9.05	9.91	10.78	11.64	12.5	13.36
0.25	0	0	0	0	0	0	0	0	0
0.75	0	0	0	0	20.83	38.66	42.97	41.61	35.4
1.25	0	0	60.94	105.71	126.38	143.3	140.73	132.83	119.34
1.75	0	101.95	172.96	212.91	228.15	243.4	233.86	218.96	198.12
2.25	103.55	212.66	282.25	316.64	326.15	338.93	322.37	300.05	271.73
2.75	209.67	320.78	388.47	416.89	420.35	429.86	406.2	376.06	340.17
3.25	313.7	426.13	491.46	513.6	510.79	516.11	485.59	447.1	403.51
3.75	415.55	528.72	591.29	607.15	597.77	597.82	560.4	513.05	461.78
4.25	515.05	628.61	688.5	697.55	680.79	674.17	630.73	574.06	515.02
4.75	0	725.71	782.18	784	760.06	744.58	696.36	630.04	563.34
5.25	0	820.83	872.71	866.9	835.2	815.11	757.36	681.11	606.98
5.75	0	0	960.06	946.1	906.01	879.89	813.8	727.46	646.24
6.25	0	0	0	1021.02	972.91	940.11	866	769.46	681.45
6.75	0	0	0	1091.51	1035.68	996.31	0	0	0
7.25	0	0	0	0	1094.58	0	0	0	0

Table 2.7: Full Scale Power Output Matrix (Capped at 858 kW)

Hs/Te	6.47	7.33	8.19	9.05	9.91	10.78	11.64	12.5	13.36
0.25	0	0	0	0	0	0	0	0	0
0.75	0	0	0	0	20.83	38.66	42.97	41.61	35.4
1.25	0	0	60.94	105.71	126.38	143.3	140.73	132.83	119.34
1.75	0	101.95	172.96	212.91	228.15	243.4	233.86	218.96	198.12
2.25	103.55	212.66	282.25	316.64	326.15	338.93	322.37	300.05	271.73
2.75	209.67	320.78	388.47	416.89	420.35	429.86	406.2	376.06	340.17
3.25	313.7	426.13	491.46	513.6	510.79	516.11	485.59	447.1	403.51
3.75	415.55	528.72	591.29	607.15	597.77	597.82	560.4	513.05	461.78
4.25	515.05	628.61	688.5	697.55	680.79	674.17	630.73	574.06	515.02
4.75	0	725.71	782.18	784	760.06	744.58	696.36	630.04	563.34
5.25	0	820.83	858	858	835.2	815.11	757.36	681.11	606.98
5.75	0	0	858	858	858	858	813.8	727.46	646.24
6.25	0	0	0	858	858	858	858	769.46	681.45
6.75	0	0	0	858	858	858	0	0	0
7.25	0	0	0	0	858	0	0	0	0

2.2.5 Power Limitations for Each Scale

The primary goal of power output limitations was to evaluate the influence of different capping strategies on the total energy generation and to facilitate standardized comparisons across

multiple scales. Limiting the power matrices in this way helps ensure consistency in the economic evaluation of wave energy systems by maintaining a uniform cost-per-watt framework. This structured analysis provides a fair comparison between full-scale, half-scale, and one-third-scale WEC configurations. A summary of power ratings and their respective scale adjustments is given in Table 2.8.

Table 2.8: Power Ratings for Each Scale

Full Scale	Half Scale	1/3 Scale
1094.58 kW	127.23 kW	34.084 kW
858 kW	63.62 kW	17.042 kW
572 kW	31.81 kW	8.521 kW
286 kW	-	-

2.2.6 Capital Costs for Scaled WEC Array Configurations

Two configurations were examined for both the half-scale and one-third-scale systems to assess the economic feasibility of deploying wave energy converters at different scales. For the half-scale case, arrays consisting of 100 and 270 WECs were modeled, arranged in 10×10 and 15×18 layouts, respectively. Structural assembly costs were scaled down using reduction factors of one-half and one-quarter of the full-scale cost, resulting in four comparison scenarios based on array size and cost scaling.

Similarly, for the one-third-scale case, arrays with 100 and 650 WECs were evaluated, arranged in 10×10 and 25×26 layouts. In this case, structural costs were reduced to one-third and one-ninth of the full-scale value, also producing four comparison cases. These configurations were developed to investigate how system scale and array size influence capital cost efficiency in wave energy converter deployments.

2.2.7 System Advisor Model (SAM) Cost Items

The System Advisor Model (SAM) is a simulation tool developed by NREL [19]. It estimates the performance and financial viability of renewable energy systems. SAM supports various technologies, including solar, wind, and wave energy. It provides outputs such as energy production, cost of energy, and payback period. Users can customize system designs and analyze different scenarios.

In this study, the System Advisor Model (SAM) is used to estimate the Levelized Cost of Energy (LCOE) for wave energy systems. By inputting mechanical power outputs from simulation data, SAM calculates the energy cost over the system's lifetime. This allows for economic comparison of different wave energy converter scales and configurations. Figure 2.8 shows the SAM interface used in this study, featuring the full-scale WEC with a rated power of 1,094.57 kW and its corresponding power matrix.

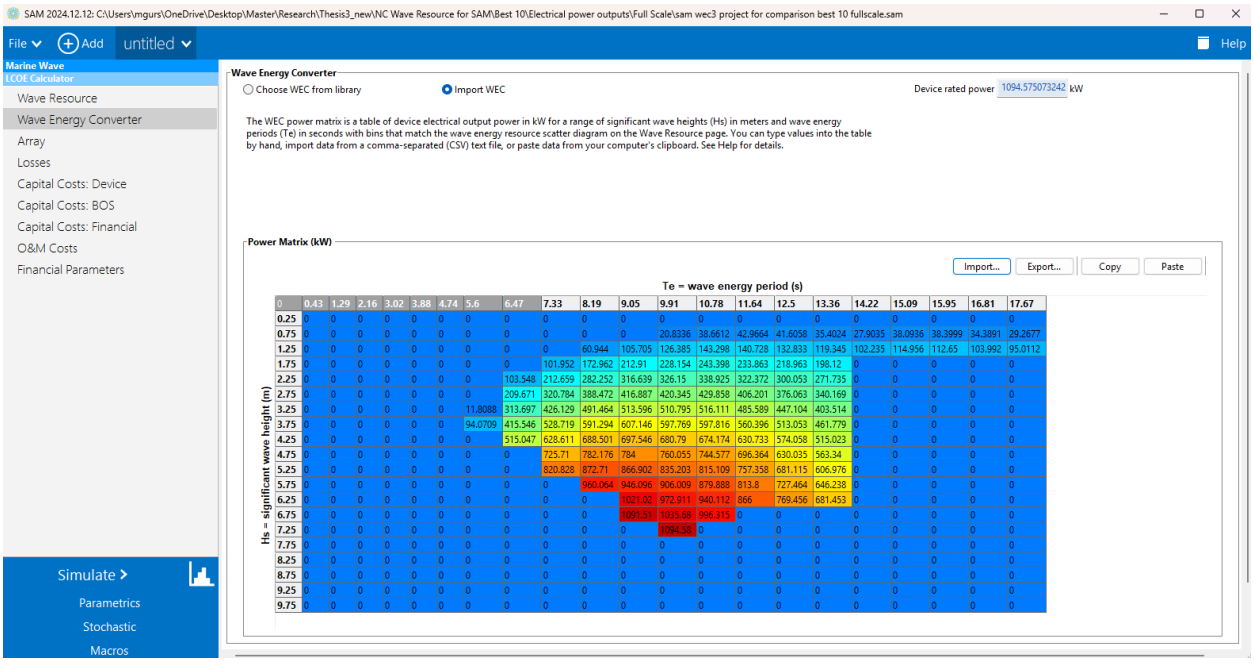

Figure 2.8: SAM interface showing full-scale WEC analysis (1,094.57 kW) with power matrix.

2.2.7.1 Array Configuration

For each WEC scale, specific array configurations were defined. The full-scale deployment used a 10 by 10 array layout. The half-scale setup included both a 10 by 10 and a 15 by 18 array configuration, while the one-by-three scale utilized a 10 by 10 and a 25 by 26 array. Regardless of scale, the spacing between devices within each row and between rows was set at 600 meters.

2.2.7.2 Loss Assumptions

System performance was adjusted to account for realistic operating conditions. Transmission losses were assumed to account for 2 percent of the total generated power, while array or device downtime contributed an additional 5 percent. Combined, these losses resulted in a total system loss of 7 percent, which was uniformly applied across all simulations.

2.2.7.3 Capital Cost Components

Capital costs were broken down into three main categories: device costs, balance of system (BOS) costs, and financial or indirect costs.

2.2.7.3.1 Device Costs

The device-related capital costs include structural assembly, power take-off (PTO) systems, and mooring foundations, with baseline full-scale values of $236,938,161 for structural assembly, $52,489,652 for the 286 kW PTO system, and $93,918,662 for the 360-kW mooring system.

To estimate the costs for different WEC scales and configurations, each component is scaled using an appropriate methodology. The structural assembly cost is scaled according to the

number of devices in the array and adjusted based on the WEC scale. This relationship is cubic due to structural volume scaling. The formula used for estimating structural costs is:

$$C_{structural} = \frac{(\frac{Structural\ Assembly\ Cost_{Full\ Scale}}{100} * Array\ Size)}{Wave\ Generator\ Scale^{Cost\ Scaling\ Exponent}} \quad (6)$$

The PTO cost is calculated proportionally to the power rating of the scaled device and multiplied by the number of devices in the array. The full-scale PTO system cost is based on a 286-kW device. The corresponding formula is:

$$C_{PTO} = \frac{(PTO\ Cost_{Full\ Scale} * \frac{Power\ Rating}{100} * Array\ Size)}{286} \quad (7)$$

The mooring cost is scaled according to the device's rated power and array size, using 360 kW as the reference power level. This approach is inspired by the taut mooring system implemented in the RM5 Wave Energy Converter (WEC) included in SAM. The mooring cost is calculated using the following formula:

$$C_{mooring} = \frac{(Mooring\ Cost_{Full\ Scale} * \frac{Power\ Rating}{100} * Array\ Size)}{360} \quad (8)$$

The total capital device cost is obtained by summing the individual scaled components as follows:

$$C_{total} = C_{structural} + C_{PTO} + C_{mooring} \quad (9)$$

This methodology ensures that capital cost estimates reflect realistic variations in system scale, device size, and array layout, enabling accurate financial analysis across different deployment scenarios.

2.2.7.3.2 Balance of System (BOS)

The balance of system costs includes the modeled fee components required for project operation. These required fees include development, engineering and management, electrical infrastructure, plant commissioning, site access, assembly and installation, and other infrastructure. These costs were based on SAM's internal modeling and scaled to match each WEC deployment scenario.

2.2.7.3.3 Financial Costs

Financial and indirect costs were considered to capture the broader scope of project development. This included a contingency budget to cover unexpected expenses, insurance costs during the construction phase, reserve accounts for financial risk management, and other financial costs commonly incurred during large-scale energy infrastructure deployment. These costs were based on SAM's internal modeling and scaled to match each WEC deployment scenario.

2.2.7.4 Operation & Maintenance Costs

Operation and maintenance (O&M) costs were estimated using the internal modeling framework provided by the System Advisor Model (SAM). These costs were scaled to align with each specific WEC deployment scenario, considering array size, device rating, and system configuration. The model incorporates typical annual servicing, inspection, and repair expenses, reflecting realistic long-term maintenance needs for wave energy systems.

2.2.7.5 Financial Parameters

Finally, a fixed charge of 10.8% rate was applied in the financial calculations. This rate encompasses the cost of capital, return on investment expectations, insurance, and other financing-

related considerations. It serves as a key factor in determining the levelized cost of energy and overall economic viability of the WEC deployment scenarios evaluated.

2.2.8 Development of Machine Learning Algorithm for Maximum Power Point Tracking

A comprehensive training dataset was developed to reflect a diverse set of realistic sea state conditions and phase shift variations to enable accurate power output prediction for Wave Energy Converters (WECs). The dataset includes wave heights ranging from 0.75 meters to 4.75 meters, incremented by 0.5 meters, yielding nine unique values. Similarly, six distinct wave periods were defined between 3.5 and 12.5 seconds, spaced at 1.8-second intervals.

For each combination of wave height and wave period, eight different time shifts were incorporated (−0.25, −0.15, −0.05, 0, 0.05, 0.15, 0.25, and 0.35 seconds) to simulate variations in the phase relationship between the wave excitation force and the device's response.

In total, 432 unique sea state scenarios were created by combining all possible values. The mechanical power output for each scenario was calculated and used to build a training dataset for machine learning-based Maximum Power Point Tracking (MPPT) in WEC systems.

CHAPTER 3: RESULTS AND DISCUSSION

3.1 ANN Configuration Analysis and MPPT Estimation Results for Wave Energy Converters

This section presents the evaluation outcomes of the tested ANN configurations and the MPPT estimation accuracy attained by the selected optimal network. The best-performing ANN configuration resulted in an error rate as low as 0.46%, underscoring the capability of machine learning in improving wave energy conversion technologies [17].

3.1.1 Regular Waves

Figures 3.1 and 3.2 present the power output results from regular wave conditions using 3D mesh grid visualizations for wave periods (T) of 6 and 10 seconds across all wave heights. Through extensive experimentation, multiple Artificial Neural Network (ANN) configurations were tested. Each configuration was trained, validated, and tested 100 times using different data splits: 70% of the data was consistently used for training, while validation percentages varied among 0%, 5%, 10%, 15%, 20%, 25%, and 30%, with the remainder allocated for testing. The tested hidden layer structures included single-layer networks with 10 and 20 neurons, and a two-layer network with [10, 10] neurons. The error rate, defined as the percentage difference between the predicted and actual output values, was calculated for each run. Among all trials, the configuration using 70% training, 0% validation, and 30% testing, paired with the [10, 10] double hidden layer, achieved the lowest individual error rate (E_r) of 0.80%, configuration performance matrix for all configurations visualized in Appendix C, with the corresponding weights provided in Appendix D [17].

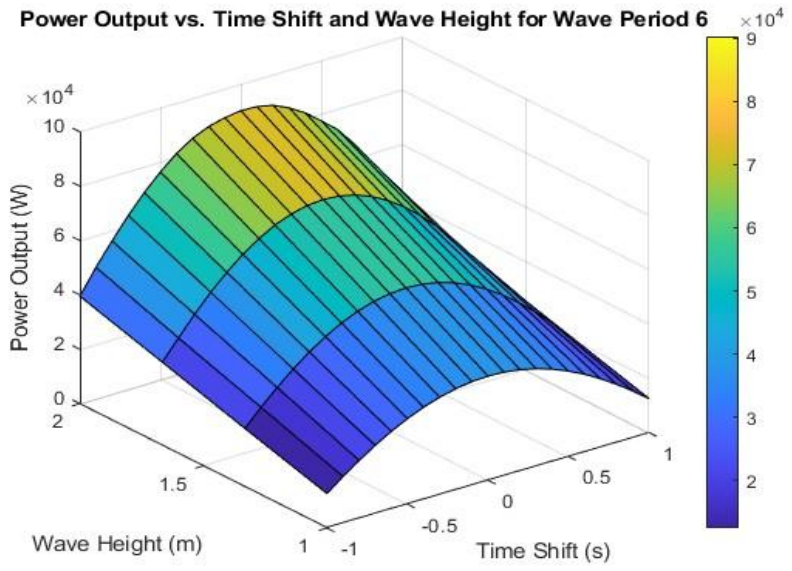

Figure 3.1: Regular wave test power outputs for T= 6 seconds [17].

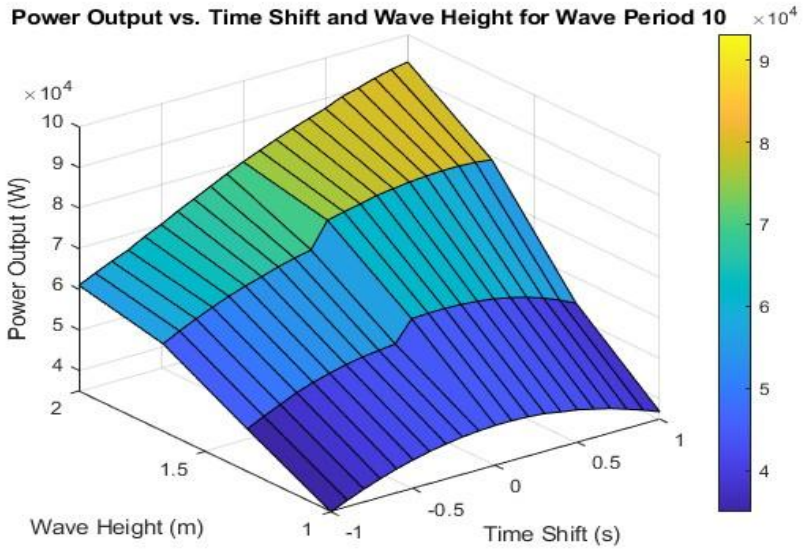

Figure 3.2: Regular wave test power outputs for T= 10 seconds [17].

A 2D heatmap was also employed to visualize and compare the average error rates (Er) across different network setups, as shown in Figure 3.3. This comparative analysis highlighted the consistency and robustness of the ANN with a using 70% training, 10% validation, and 20% testing, paired with the single hidden layer with 20 neuron architecture, which demonstrated the

best overall performance across all 100 runs in handling the complex dynamics of ocean wave energy conversion [17].

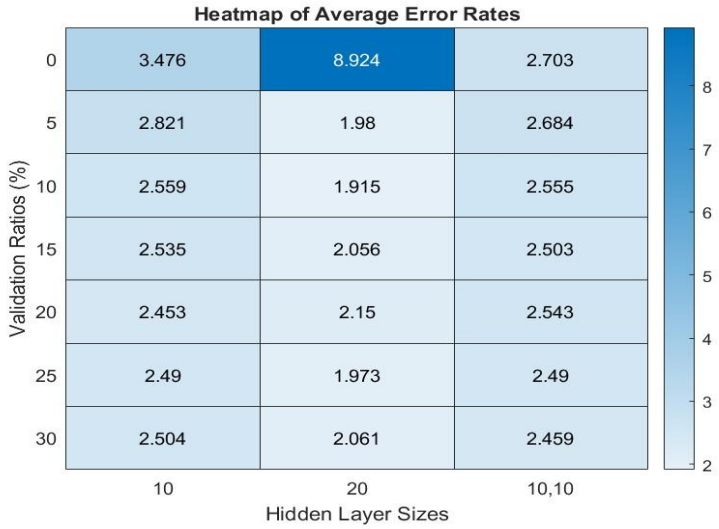

Figure 3.3: Average error rate (E_r) heatmap for a regular wave case, averaged by hidden layer size and validation ratio [17].

Once the most accurate ANN architecture was determined, the model predicted maximum power outputs for randomly generated sea states. This dataset included five wave heights (1.2071 m, 1.406 m, 1.6723 m, 1.7168 m, and 1.9560 m) and five wave periods (6.2062 s, 7.6394 s, 8.3253 s, 8.8038 s, and 9.8532 s), resulting in 25 distinct testing scenarios. The ANN consistently delivered high-accuracy predictions, achieving an average error rate of just 0.09% and a maximum error of 0.73%. These results highlight the strength of ANN-based methods in improving Maximum Power Point Tracking (MPPT) for Wave Energy Converter (WEC) Power Take-Off (PTO) systems. Overall, this study supports using neural networks as a powerful tool to enhance the performance and reliability of wave energy technologies in practical applications [17].

3.1.2 Irregular Waves

Figures 3.4 and 3.5 display sample datasets of power output under irregular wave conditions, corresponding to peak periods (T_p) of 7 and 11 seconds, respectively, and covering a

range of significant wave heights (H_{m0}). The results are visualized using 3D mesh grid plots. The configuration that used 70% of the data for training and 30% for testing, with double hidden layers containing 10 neurons each, achieved the lowest recorded error rate of 0.46%, configuration performance matrix for all configurations visualized in Appendix C, with the corresponding weights provided in Appendix D. The error distribution for this optimal model is shown in the histogram in Figure 3.7 [17].

Figure 3.4: Irregular wave test power outputs for T= 7 seconds [17].

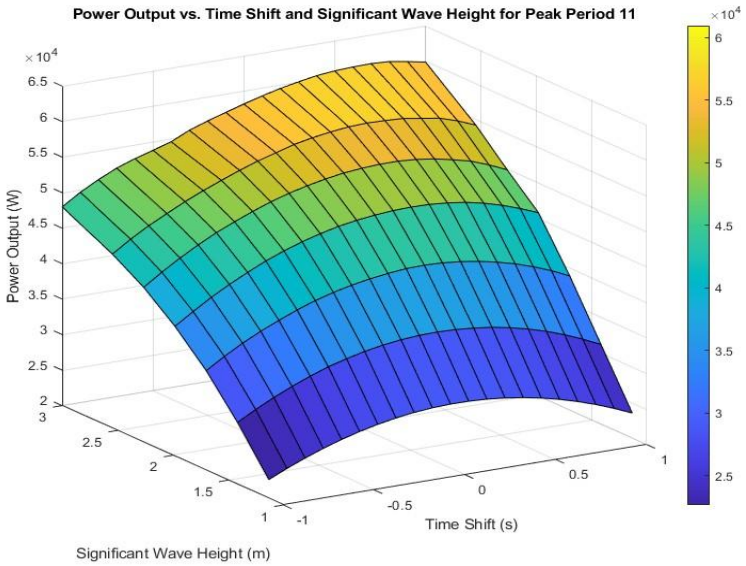

Figure 3.5: Irregular wave test power outputs for T= 11 seconds [17].

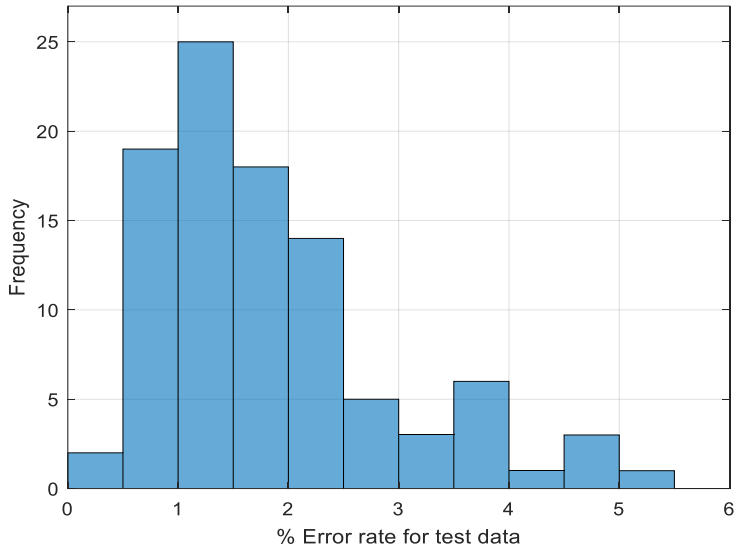

Figure 3.6: Error rate (E_r) histogram for the double hidden layer topology (94% population) [17].

Although the configuration that used 70% of the data for training and 30% for testing, with two hidden layers containing 10 neurons in each layer, did not yield the lowest average error rate across all experiments, it demonstrated excellent estimation performance within its configuration. The optimal ANN structure was determined through systematic tuning of architectural, training process, and evaluation methods, resulting in strong generalization over the tested parameter space [17].

A 2D heatmap was generated to illustrate the error rates (E_r) across all tested setups, enabling performance comparison of different ANN configurations. Figure 3.7 shows how the configurations in hidden layer sizes and validation ratios affect the prediction accuracy. Across all runs, the configuration with 70% training, 0% validation, and 30% testing, using a single hidden layer with 10 neurons, achieved the lowest overall average error rate, demonstrating the most consistent and accurate performance in modeling the WEC system [17].

Figure 3.7: An example irregular wave case for an average Error Rate (E_r) 2D heatmap [17].

The best performing "double hidden layer" ANN configuration was used to estimate maximum power outputs. This process involved evaluating 25 unique scenarios, each representing a combination of five significant wave heights (1.2322 m, 1.3741 m, 2.1232 m, 2.5874 m, and 2.8767 m) and five peak periods (6.0714 s, 6.9731 s, 8.0227 s, 8.8163 s, and 9.4129 s). The resulting estimations demonstrated high accuracy, with an average error rate of 0.14% and a maximum of 0.95%. Figure 3.8 presents the error margins between predicted and actual power outputs for these irregular wave conditions, mapped over the tested H_{m0} and T_p values [17].

These results validate the effectiveness of ANN-based approaches in improving Maximum Power Point Tracking (MPPT) strategies for Wave Energy Converter–Power Take-Off (WEC–PTO) systems. The study demonstrates the potential of artificial neural networks to significantly improve the performance, reliability, and efficiency of wave energy conversion technologies in real-world environments [17].

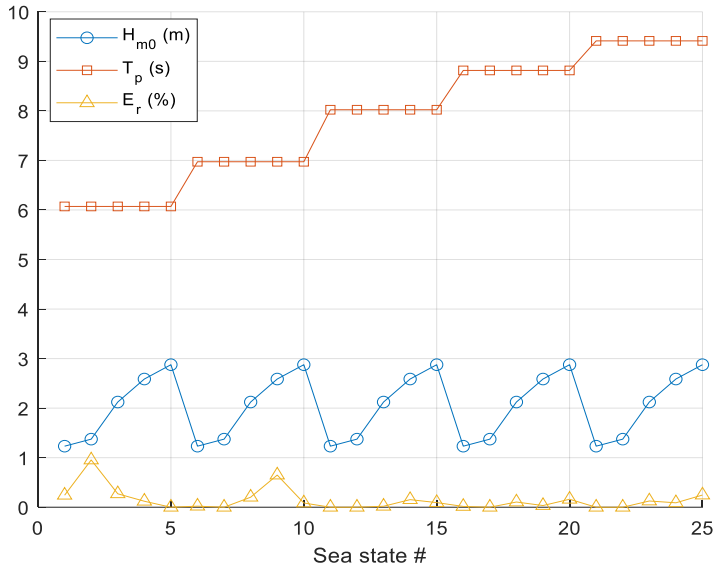

Figure 3.8: MPPT performance with randomized twenty-five sea states [17].

3.2 Analysis of LCOE for Scaled Wave Energy Converter Systems

While the machine learning-based MPPT estimation results presented in Section 3.1 were derived using a hypothetical Wave Energy Converter (WEC) and sea states, further analysis is necessary to evaluate the practical applicability of this approach. To address this, Section 3.2 explores the integration of the proposed method with a more realistic WEC model, specifically adapted for the wave conditions along the North Carolina coast. This analysis also considers system scaling and cost optimization by examining the Levelized Cost of Energy (LCOE) for different WEC configurations.

The analysis begins by comparing the benchmark RM3-WEC heaving buoy, which operates with passive damping control, to a full-scale slider-crank WEC utilizing reactive control, to assess potential performance gains. As illustrated in Figures 3.12 and 3.13, the slider-crank model achieves an approximate 30% reduction in Levelized Cost of Energy (LCOE) and a 6.2% increase in capacity factor, highlighting its enhanced efficiency. Further comparisons are made among the full-scale, half-scale, and one-third-scale versions of the slider-crank WEC, assuming a standardized 10 × 10 array configuration. These results were obtained using the five most frequently occurring sea sites, as identified in Table 2.3—specifically, sea sites 169, 164, 157, 142 and 127 for the full-scale system, sea sites 127, 142, 135, 157, and 150 for the half-scale system, and sea sites 127, 142, 169, 157, and 164 for the one-third-scale system. Full-Scale WEC system, with a rated capacity of 286 kW, achieves the lowest Levelized Cost of Energy (¢/kWh) among its configurations. Half-scale WEC system, with a rated capacity of 63.62 kW, achieves the lowest Levelized Cost of Energy (¢/kWh) among its configurations. The one-third-scale system achieves its lowest LCOE with a rated capacity of 17.0 kW, achieves the lowest Levelized Cost of Energy (¢/kWh) among its configurations. A detailed comparison of the capacity factor and cost of energy

values is visualized in Figures 3.9, 3.10 and 3.11 for the full-scale, half-scale and one-third-scale systems, respectively. Figures 3.14 and 3.15 show that the half scaled WEC system has the lowest Levelized Cost of Energy (¢/kWh) among all scaled systems.

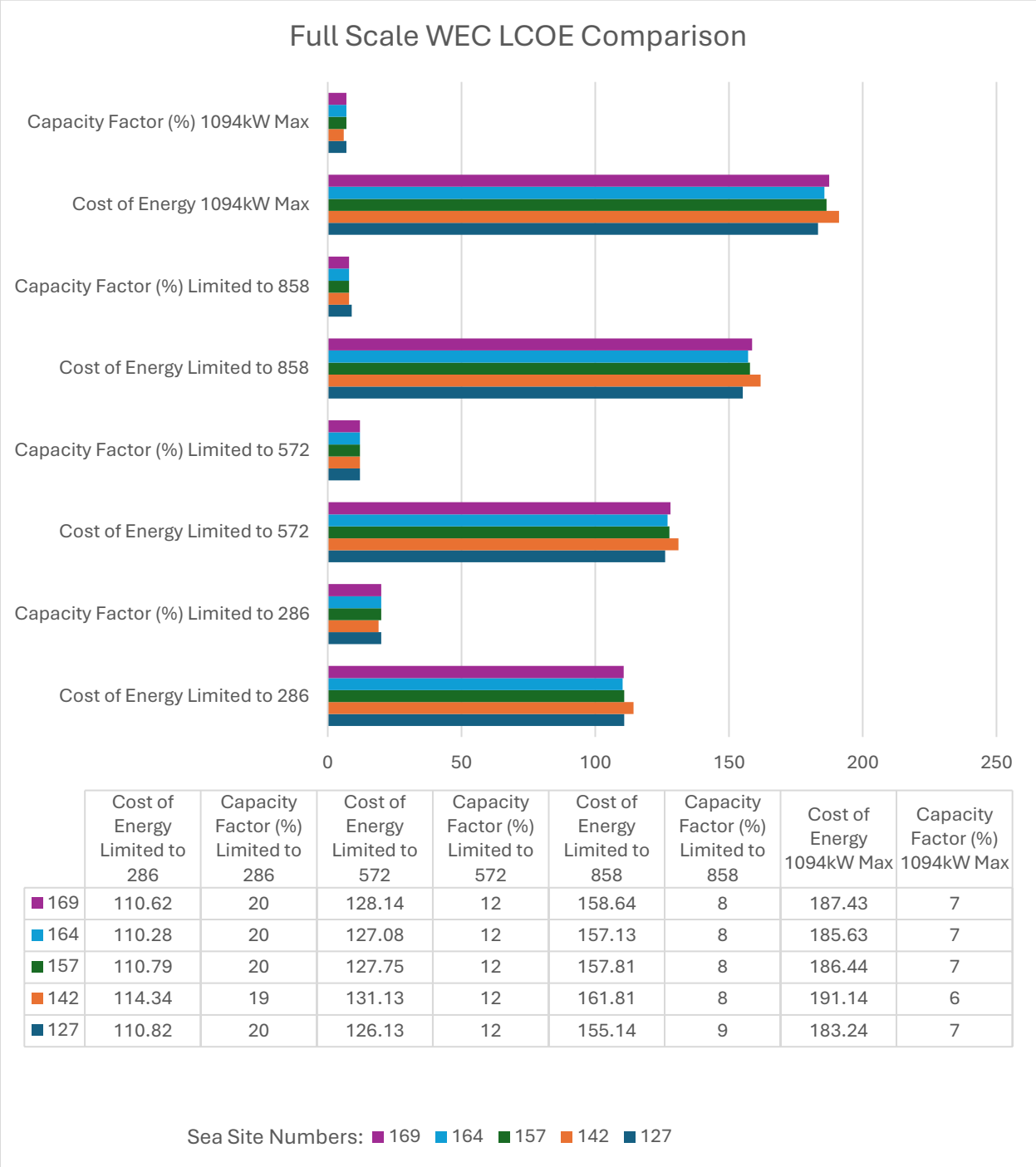

	Cost of Energy Limited to 286	Capacity Factor (%) Limited to 286	Cost of Energy Limited to 572	Capacity Factor (%) Limited to 572	Cost of Energy Limited to 858	Capacity Factor (%) Limited to 858	Cost of Energy 1094kW Max	Capacity Factor (%) 1094kW Max
169	110.62	20	128.14	12	158.64	8	187.43	7
164	110.28	20	127.08	12	157.13	8	185.63	7
157	110.79	20	127.75	12	157.81	8	186.44	7
142	114.34	19	131.13	12	161.81	8	191.14	6
127	110.82	20	126.13	12	155.14	9	183.24	7

Figure 3.9: Full Scale WEC LCOE Comparison.

	Cost of Energy 127.23 kW Max	Capacity Factor 127.23 kW Max	Cost of Energy Limited to 63.62 kW	Capacity Factor Limited to 63.62 kW	Cost of Energy Limited to 31.81 kW	Capacity Factor Limited to 31.81 kW
157	73.52	26	58.13	48	65.98	70
150	75.46	25	59.59	47	67.37	69
142	74.32	25	58.82	48	66.69	69
135	75.26	25	59.49	47	67.24	69
127	74.01	26	58.65	48	66.59	69

Figure 3.10: Half Scaled WEC LCOE Comparison.

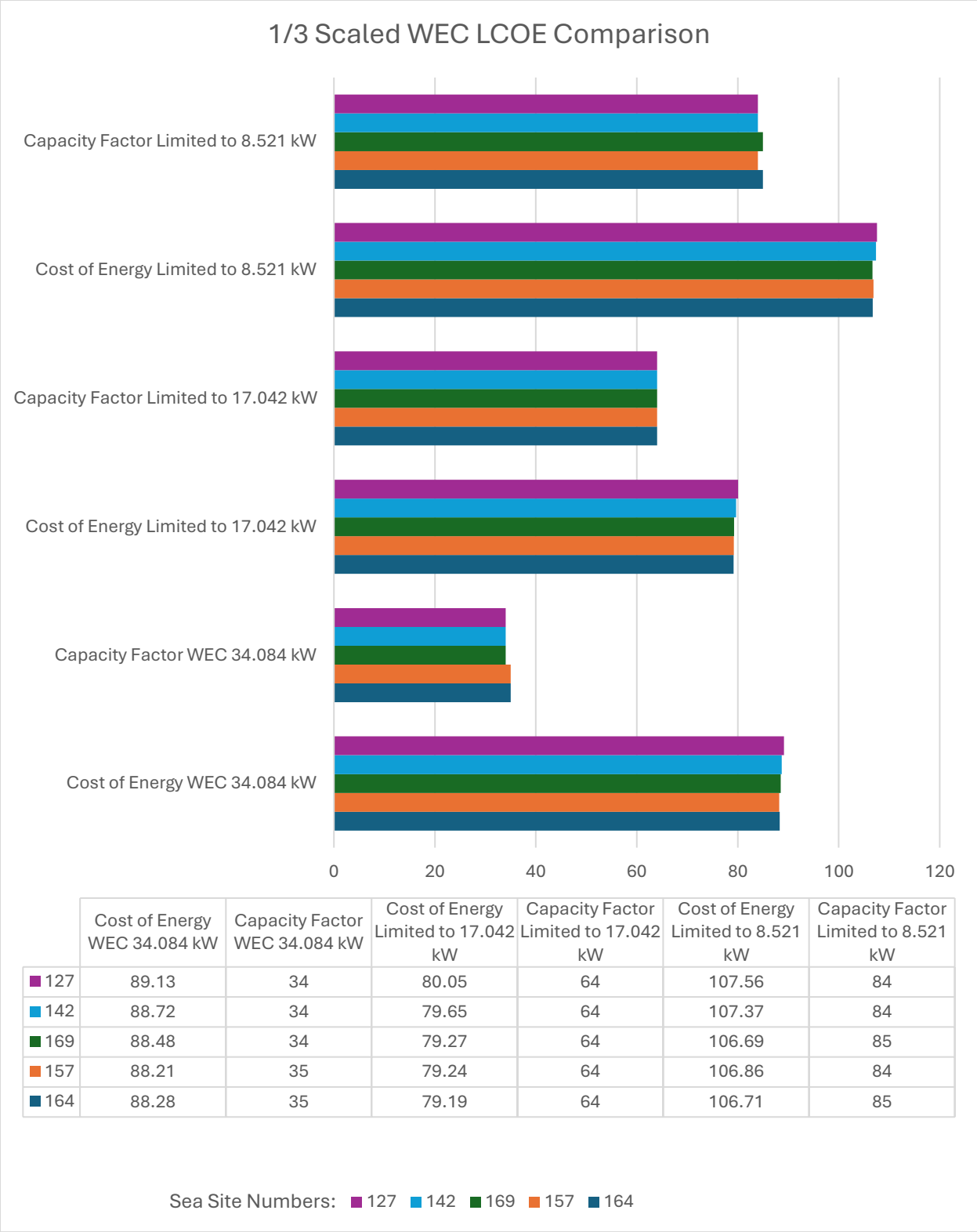

	Cost of Energy WEC 34.084 kW	Capacity Factor WEC 34.084 kW	Cost of Energy Limited to 17.042 kW	Capacity Factor Limited to 17.042 kW	Cost of Energy Limited to 8.521 kW	Capacity Factor Limited to 8.521 kW
127	89.13	34	80.05	64	107.56	84
142	88.72	34	79.65	64	107.37	84
169	88.48	34	79.27	64	106.69	85
157	88.21	35	79.24	64	106.86	84
164	88.28	35	79.19	64	106.71	85

Figure 3.11: 1/3 Scaled WEC LCOE Comparison.

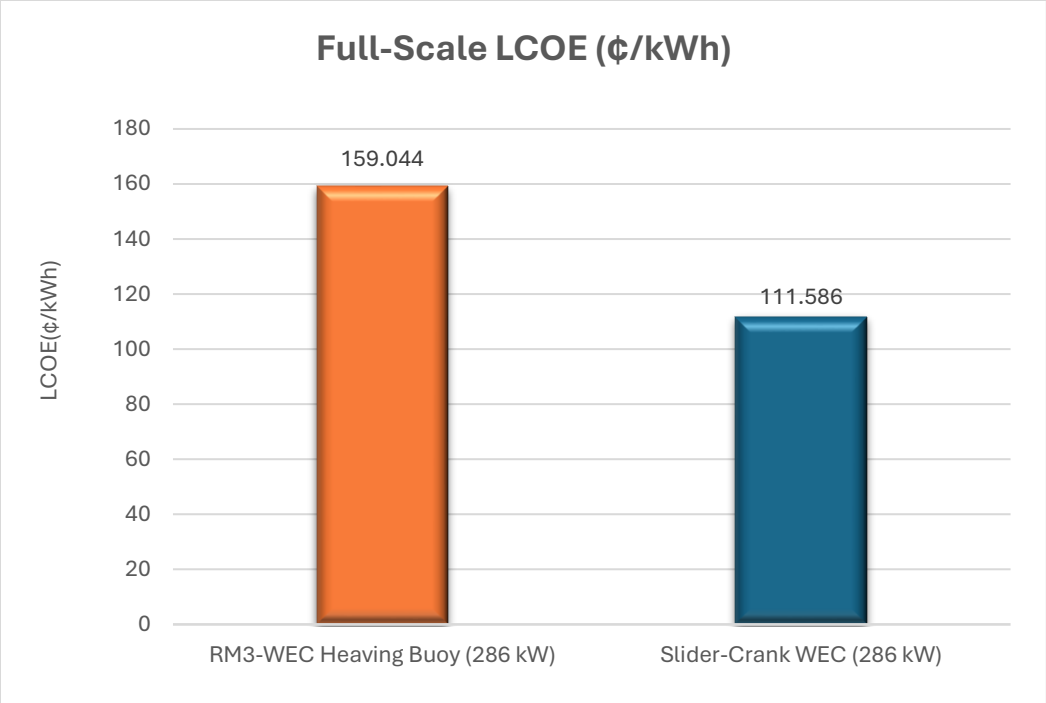

Figure 3.12: Levelized Cost of Energy (LCOE) at Full Scale (¢/kWh).

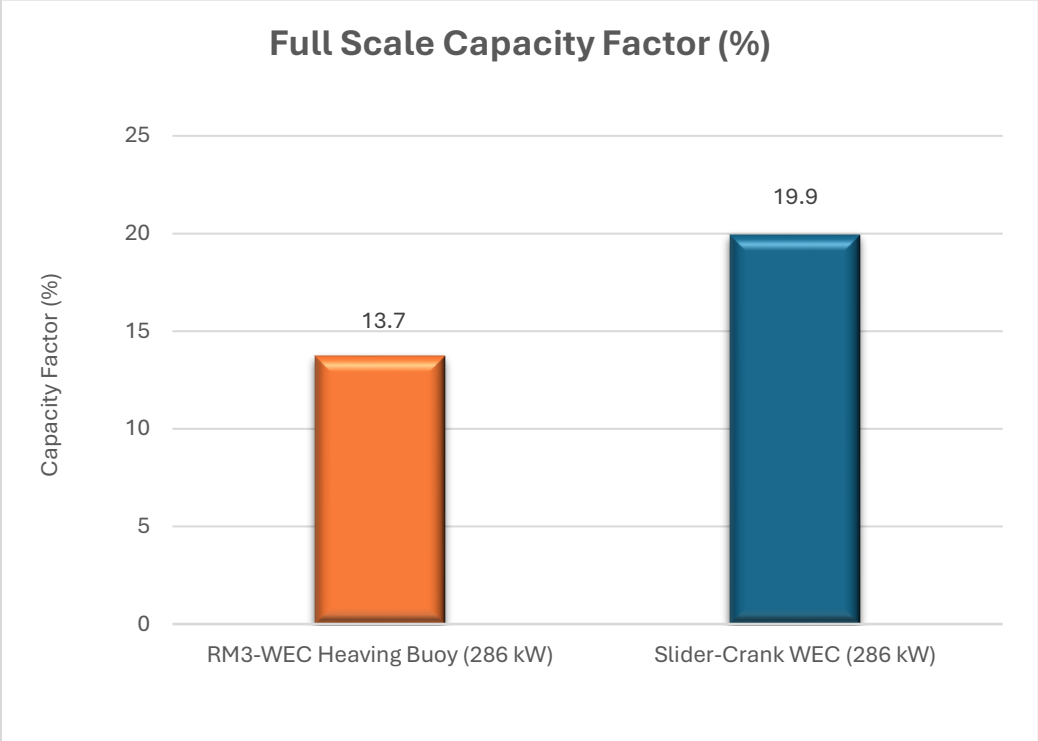

Figure 3.13: Capacity Factor at Full Scale (%).

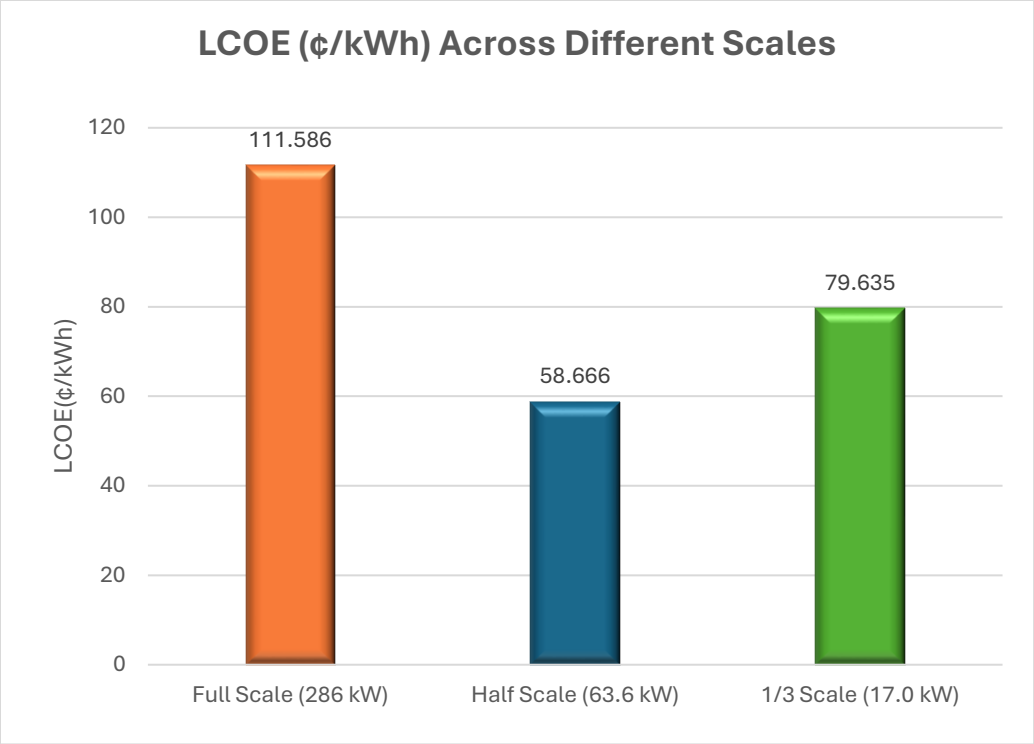

Figure 3.14: Levelized Cost of Energy (LCOE) Comparison Across Different Scales (¢/kWh).

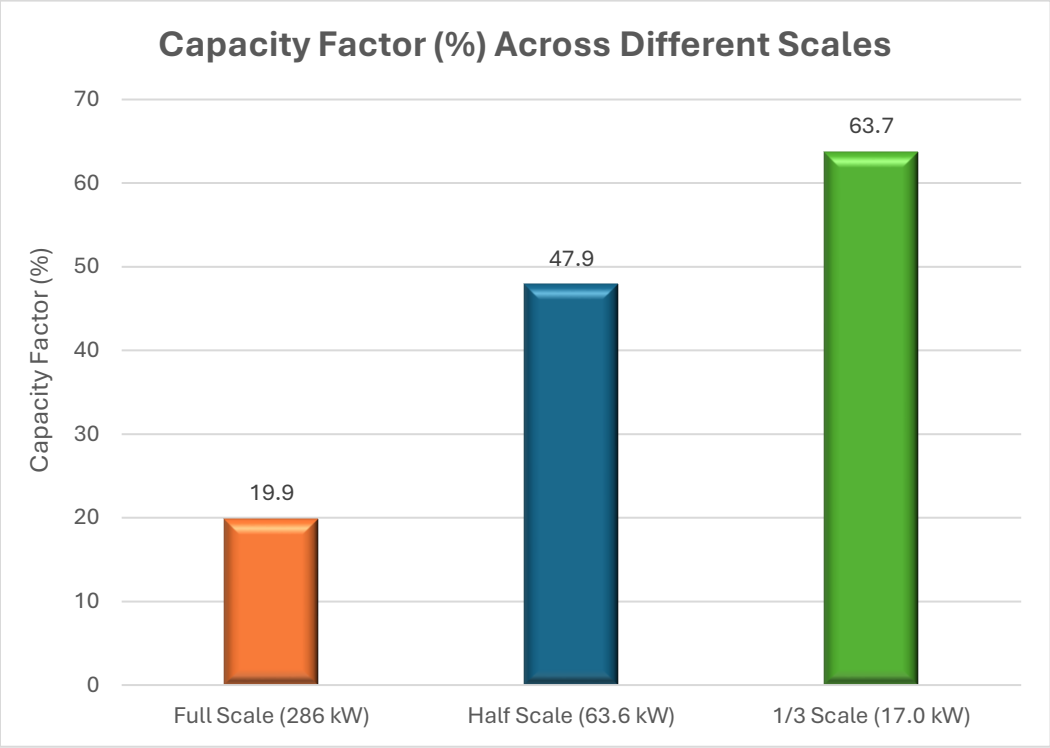

Figure 3.15: Capacity Factor Comparison Across Different Scales (%).

The study also investigates the effects of varying array configurations on LCOE and capacity factors. The half-scale WEC was analyzed under two array configurations: 10 × 10 and 15 × 18. Likewise, the one-third-scale WEC was compared with 10 × 10 and 25 × 26 arrays, as presented in Figures 3.16 and 3.17. These comparisons were conducted to ensure consistent performance and cost assessment across different array sizes.

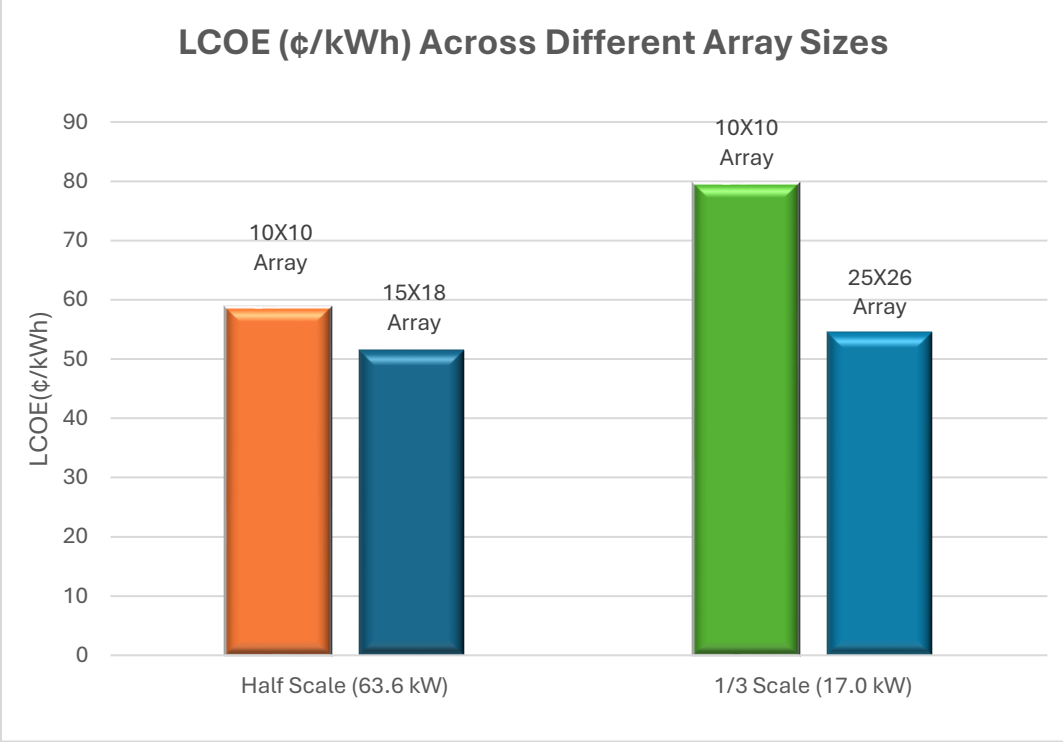

Figure 3.16: Levelized Cost of Energy (LCOE) Comparison Across Different Array Sizes (¢/kWh).

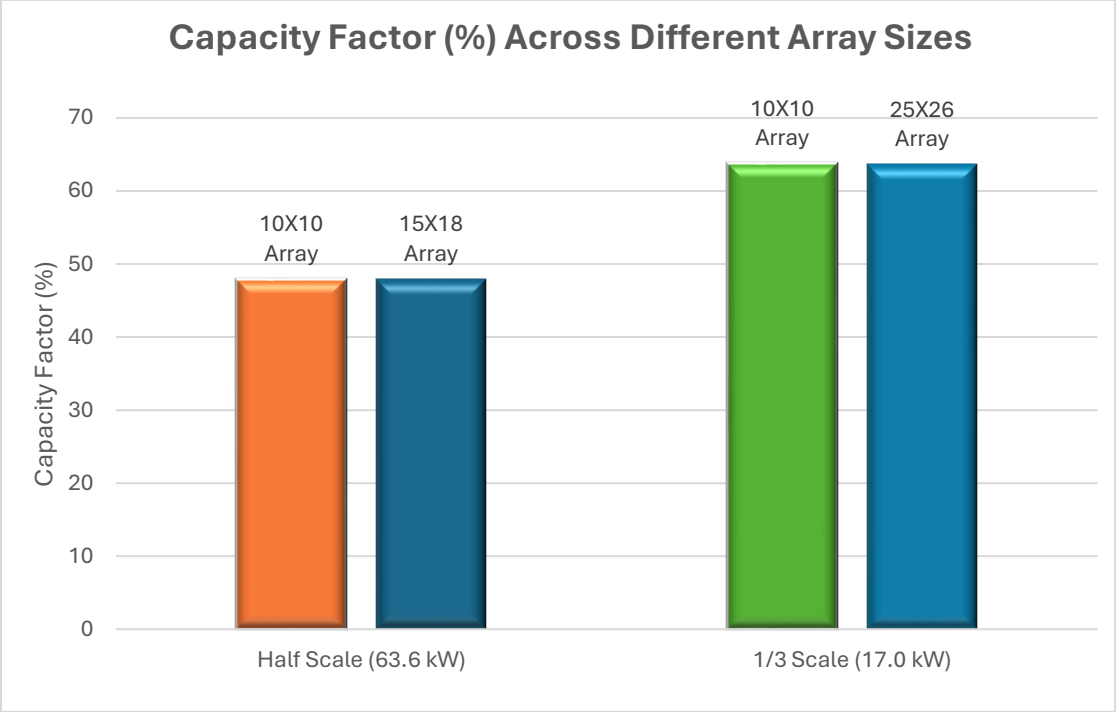

Figure 3.17: Capacity Factor Comparison Across Different Array Sizes (%).

The reference configuration for the full-scale WEC comprises a 10 × 10 array, delivering approximately 12.4 MW of average mechanical power output (based on 100 devices rated at 124 kW each). To match this output at smaller scales, the number of devices must be increased proportionally according to the power output outlined in Table 2.4. For the half-scale WEC, this requirement translates into a 15 × 18 array, while the one-third-scale system requires a 25 × 26 array.

This scaling adjustment has a significant impact on cost metrics. In particular, the one-third-scale configuration exhibited a substantial 32% reduction in LCOE, while the resulting change in capacity factor was minimal. The one-half-scale configuration exhibited also a notable 12.3% reduction in LCOE, as reflected in Figure 3.16, while the resulting change in capacity factor was minimal as visualized in Figure 3.17.

3.3 Development of Machine Learning Algorithm for Maximum Power Point Tracking

The Levelized Cost of Energy (LCOE) comparison across different scales showed that the half-scale slider-crank WEC achieved the lowest LCOE, at 58.67 ¢/kWh, outperforming all other scaled configurations. To support this analysis, a comprehensive training dataset was developed to reflect a broad range of realistic sea state conditions and time shift variations, allowing for a thorough evaluation and further cost reduction of the half-scale WEC's performance.

Wave heights were selected in 0.5-meter intervals, ranging from 0.75 to 4.75 meters, resulting in nine distinct height values. Similarly, wave periods ranged from 3.5 to 12.5 seconds in 1.8-second increments, yielding six unique period values. Each combination of wave height and wave period was further paired with eight time shift values: −0.25, −0.15, −0.05, 0, 0.05, 0.15, 0.25, and 0.35 seconds. These time shifts were introduced to simulate varying phase alignments between the wave excitation force and the WEC's dynamic response.

The selected wave height and period ranges were based on Joint Probability Distribution (JPD) analysis of the target sites, covering over 96% of observed sea states. This ensures that the dataset reflects the most representative ocean conditions, providing a reliable foundation for training and validating machine learning models.

Combining all wave heights, periods, and time shifts resulted in a total of 432 distinct sea state scenarios. For each scenario, the mechanical power output was calculated to create a robust dataset for training ANN models to predict the half scaled WEC's performance under dynamic ocean conditions.

Figures 3.19 - 3.25 present power output results for time shifts of −0.35, −0.25, −0.15, −0.05, 0, 0.05, 0.15 and 0.25 seconds, respectively, demonstrating the impact of phase alignment on energy extraction efficiency. It can be seen from these figures that a time shift of -0.05 seconds was the best performer overall.

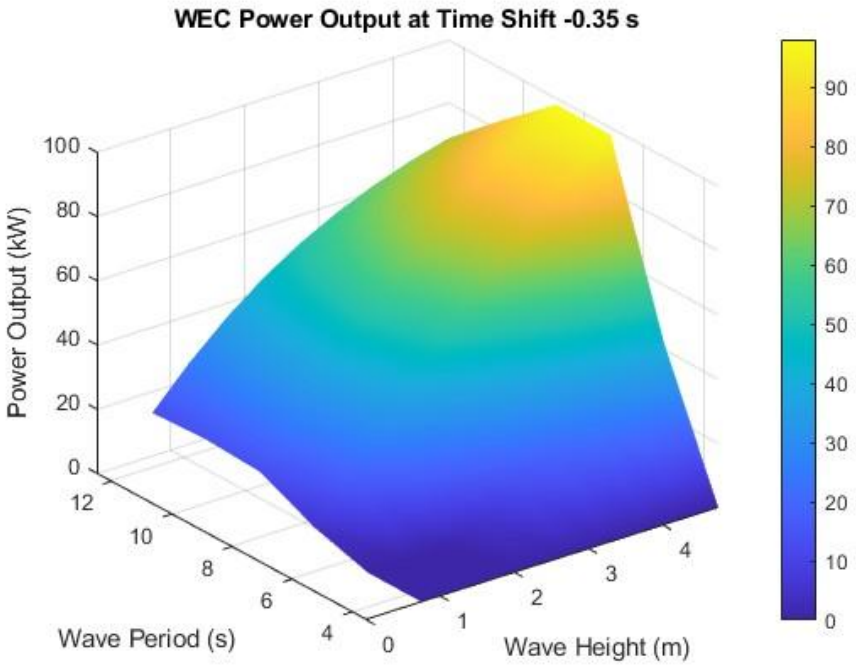

Figure 3.18: 3D plot of WEC power output at a time shift of -0.35 seconds.

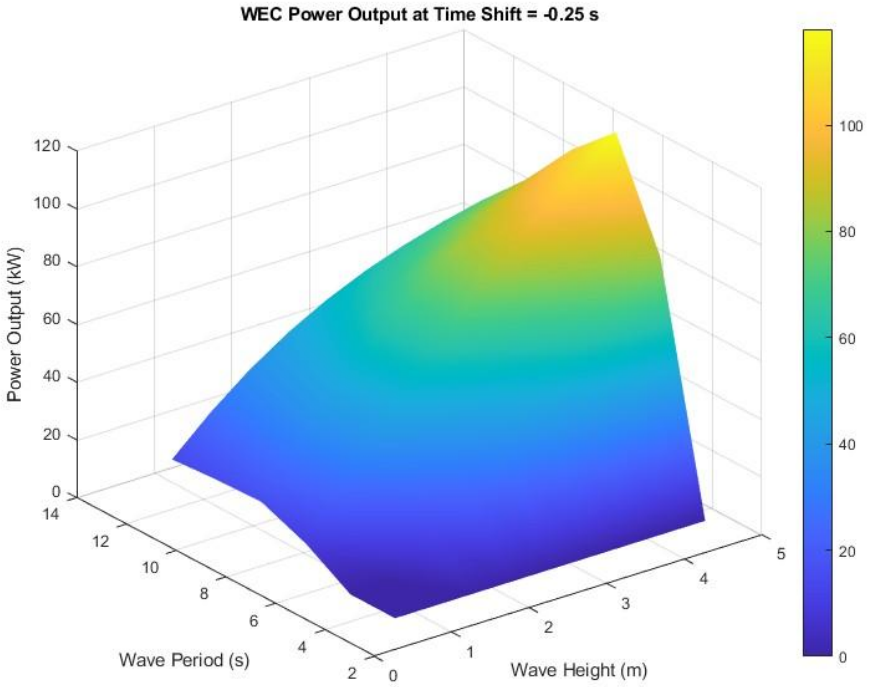

Figure 3.19: 3D plot of WEC power output at a time shift of -0.25 seconds.

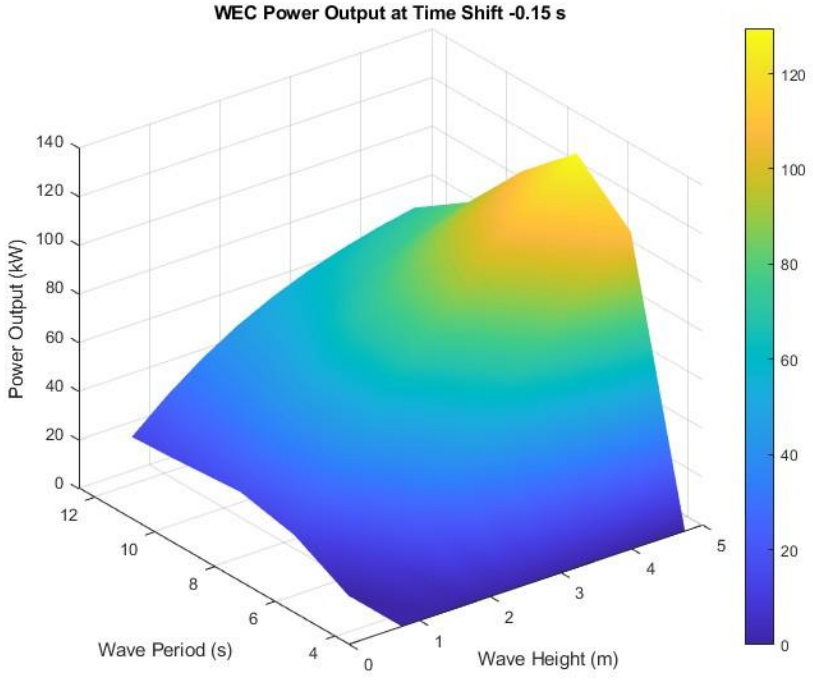

Figure 3.20: 3D plot of WEC power output at a time shift of -0.15 seconds.

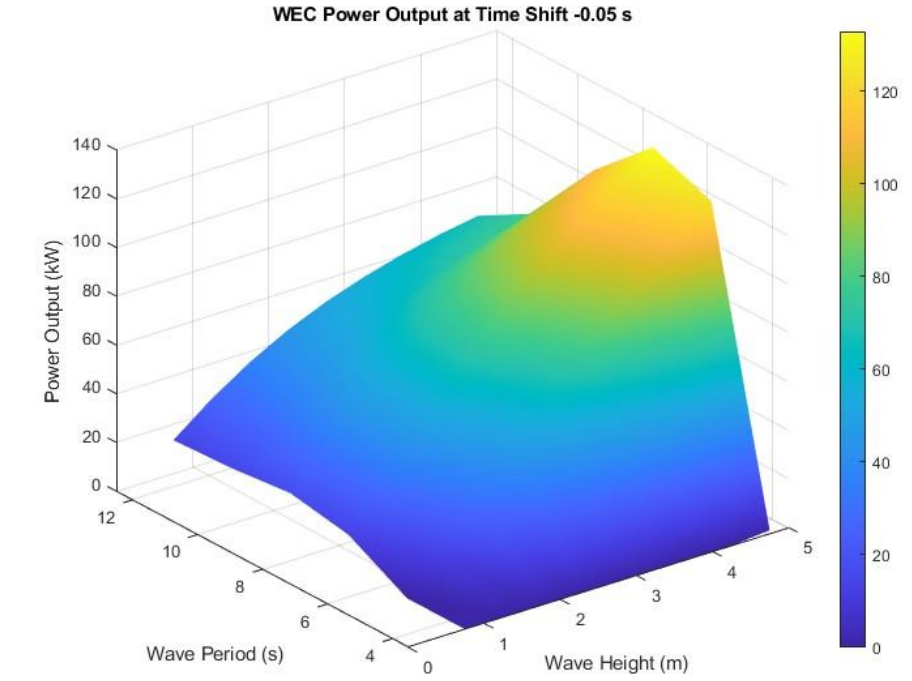

Figure 3.21: 3D plot of WEC power output at a time shift of -0.05 seconds.

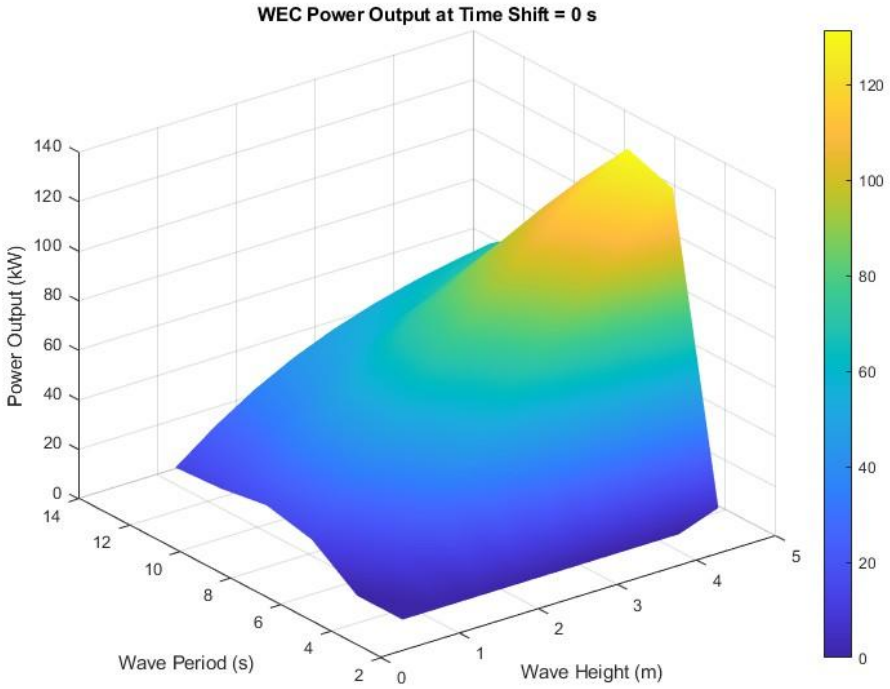

Figure 3.22: 3D plot of WEC power output at a time shift of 0 second.

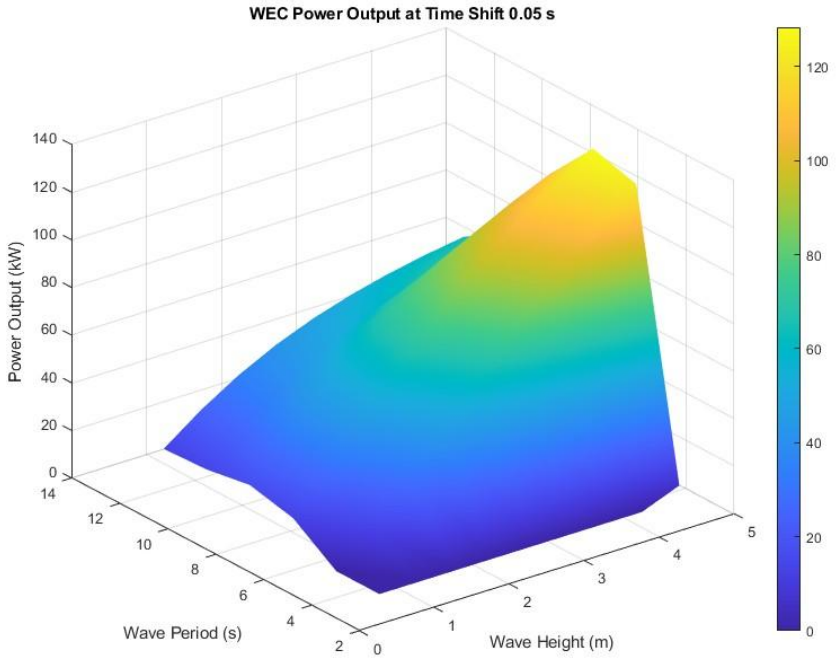

Figure 3.23: 3D plot of WEC power output at a time shift of 0.05 seconds.

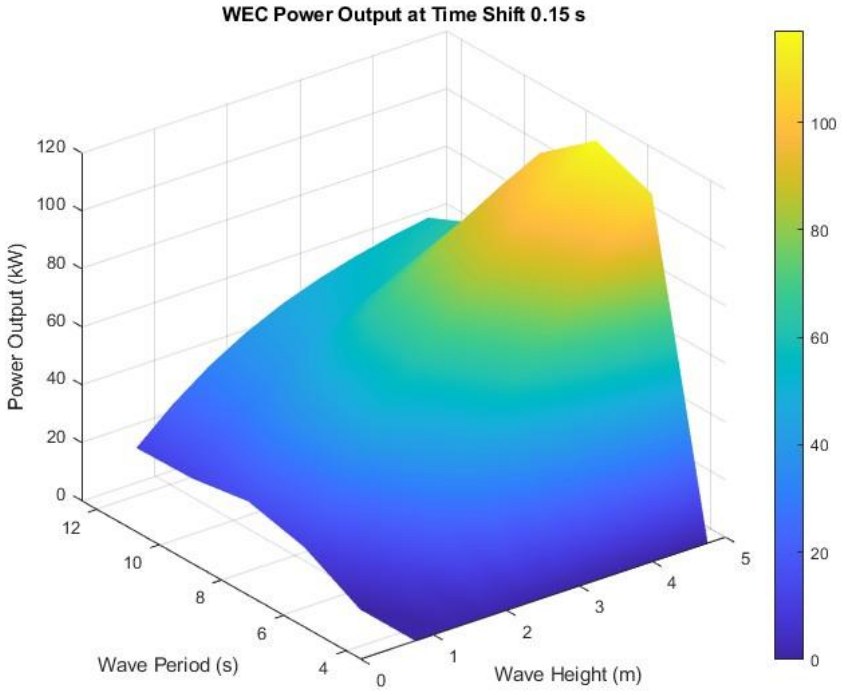

Figure 3.24: 3D plot of WEC power output at a time shift of 0.15 seconds.

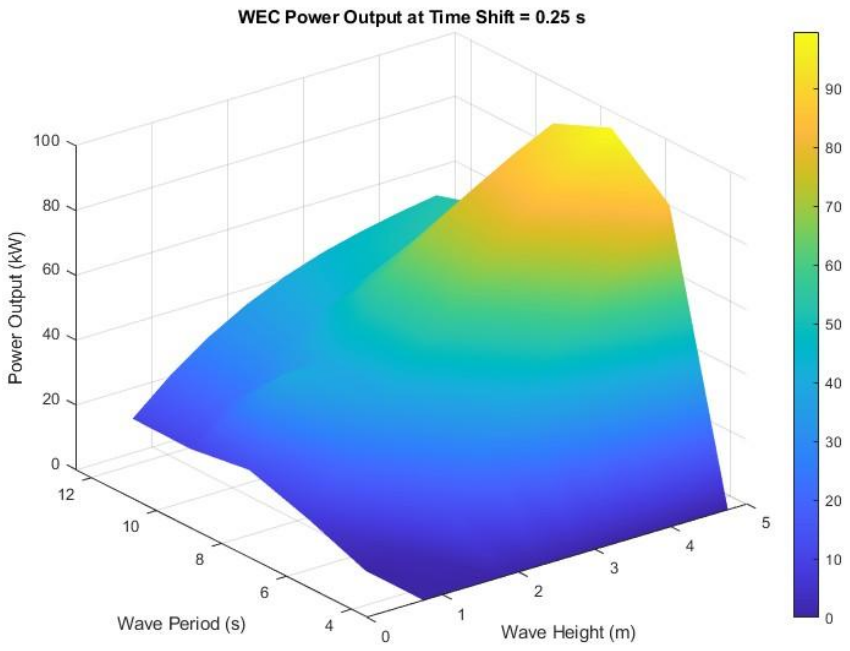

Figure 3.25: 3D plot of WEC power output at a time shift of 0.25 seconds.

CHAPTER 4: CONCLUSIONS & FUTURE WORK

This thesis investigates various Artificial Neural Network (ANN) topologies and training configurations to develop a Maximum Power Point Tracking (MPPT) method for a WEC-PTO system. The trained ANNs were tested using randomized sea states and demonstrated an error rate below 1%, confirming that machine learning is an effective tool for renewable energy applications—particularly for Wave Energy Converters (WECs). Following this analysis, the Levelized Cost of Energy (LCOE) was calculated to compare the economic performance of two WEC types: the benchmark RM3-WEC Heaving Buoy and the Slider-Crank WEC. The study then focused on the more cost-effective Slider-Crank design, evaluating it at three scales—full, half, and one-third. Once the half-scale Slider-Crank WEC was identified as having the lowest LCOE, power outputs under different time shift conditions were calculated and used for further machine learning analysis.

Future work includes evaluating the Slider-Crank WEC model using more practical mooring configurations and stiffness values to improve performance. The results need to be analyzed in six degrees of freedom (6DOF), allowing for a comprehensive understanding of the WEC's dynamic response in all translational (surge, sway, heave) and rotational (roll, pitch, yaw) motions. This analysis provides a more robust evaluation of the system's behavior and ability to extract energy effectively under varying sea conditions.

Future work also needs to focus on developing and validating an Artificial Neural Network (ANN) to enable real-time Maximum Power Point Tracking (MPPT). The training dataset, comprising 432 unique sea state scenarios defined by combinations of wave height, wave period, and time shift, should be used to train and test multiple ANN configurations. Various architectures

should be explored by adjusting hidden layer sizes, activation functions, and learning algorithms to identify the most effective model.

The dataset needs to be divided into training, validation, and testing sets to ensure generalization and minimize overfitting. Once the optimal ANN structure is identified, it needs to be used to estimate WEC power output under diverse and unseen sea conditions. The trained model should be further assessed for its responsiveness and suitability for real-time control applications.

REFERENCES

[1] Gilland, B. (1995). World Population, Economic Growth, and Energy Demand, 1990-2100: A Review of Projections. *Population and Development Review*, *21*(3), 507–539. https://doi.org/10.2307/2137748

[2] Jaramillo, P., & Muller, N. Z. (2016). Air pollution emissions and damages from energy production in the U.S.: 2002–2011. *Energy Policy*, *90*, 202–211. https://doi.org/10.1016/j.enpol.2015.12.035

[3] Bilgen, S., Kaygusuz, K., & Sari, A. (2004). Renewable Energy for a Clean and Sustainable Future. *Energy Sources*, *26*(12), 1119–1129. https://doi.org/10.1080/00908310490441421

[4] Marsh, J. (2023, July 5). *Renewable energy: All about clean power*. Energysage. https://www.energysage.com/about-clean-energy/

[5] Union of Concerned Scientists. (2017, December 20). *Benefits of renewable energy use*. https://www.ucs.org/resources/benefits-renewable-energy-use

[6] Kuo, G. (2019, May). *When fossil fuels run out, what then?* Millennium Alliance for Humanity and the Biosphere (MAHB), Stanford University. https://mahb.stanford.edu/library-item/fossil-fuels-run/

[7] Lumley, G. (2025, March). *What is wave power?* BKV Energy. https://bkvenergy.com/learning-center/what-is-wave-energy/

[8] U.S. Government Accountability Office. (2021, June 9). *Science & tech spotlight: Renewable Ocean Energy* (GAO-21-533SP). https://www.gao.gov/products/gao-21-533sp

[9] Meadow, S. (2023, November 6). *The untapped potential of wave energy: A sustainable future ahead*. The Renewables. https://therenewables.org/potential-of-wave-energy/

[10] Liu, Z., Wang, J., Tao, T., Zhang, Z., Chen, S., Yi, Y., Han, S., & Liu, Y. (2023). Wave power prediction based on seasonal and trend decomposition using locally weighted scatterplot smoothing and dual-channel Seq2Seq model. *Energies*, *16*(22), 7515. https://doi.org/10.3390/en16227515

[11] Li, L., Yuan, Z.-M., & Gao, Y. (2018). Maximization of energy absorption for a wave energy converter using the deep machine learning. *Energy*, *165*, 340–349. https://doi.org/10.1016/j.energy.2018.09.093

[12] Saulnier, J.; Ricci, P.; Clément, A.; de O. Falcao, A. (2009). Mean Power Output Estimation of WECs in Simulated Sea. Paper presented at 8th European Wave and Tidal Energy Conference (EWTEC 2009), Uppsala, Sweden.

[13] Sang, Y., Karayaka, H. B., Yan, Y., Zhang, J. Z., Muljadi, E., & Yu, Y.-H. (2015). Energy extraction from a slider-crank wave energy converter under irregular wave conditions. In *OCEANS 2015 - MTS/IEEE Washington* (pp. 1–7). IEEE. https://doi.org/10.23919/OCEANS.2015.7401873

[14] Hasselmann, K., Barnett, T., Bouws, E., Carlson, H., Cartwright, D., Enke, K., Ewing, J., Gienapp, H., Hasselmann, D., Kruseman, P., Meerburg, A., Muller, P., Olbers, D., Richter, K., Sell, W., & Walden, H. (1973). Measurements of wind-wave growth and swell decay during the Joint North Sea Wave Project (JONSWAP). *Deutsche Hydrographische Zeitschrift, 8*, 1–95.

[15] MathWorks Help Center. (2025, April 13). *Divide data for optimal neural network training*. Available online: https://www.mathworks.com/help/deeplearning/ug/divide-data-for-optimal-neural-network-training.html

[16] MathWorks Help Center. (2025, April 13). *trainlm: Levenberg-Marquardt backpropagation*. Available online: https://www.mathworks.com/help/deeplearning/ref/trainlm.html

[17] Gursel, O., Yanik, P., & Karayaka, H. (2024, October 13). *Integration of Machine Learning for Enhanced Wave Energy Converter Power Output Estimation* (pp. 1–6). https://doi.org/10.1109/NAPS61145.2024.10741837

[18] Sandia National Laboratories. (2025, January 20). *Reference Model 3 (RM3) Scaled Geometry: Wave Point Absorber* [Dataset]. Data.gov. https://catalog.data.gov/dataset/reference-model-3-scaled-geometry-rm3-wave-point-absorber-55f0a

[19] System Advisor Model™ Version 2024.12.12 (SAM™ 2024.12.12). National Renewable Energy Laboratory. Golden, CO. Accessed April 19, 2025. https://sam.nrel.gov/download/version-2024-12-12.html

[20] Karayaka, H.B.; Yu, Y.-H.; Muljadi, E. Investigations into Balancing Peak-to-Average Power Ratio and Mean Power Extraction for a Two-Body Point-Absorber Wave Energy Converter. *Energies* 2021, 14, 3489. https://doi.org/10.3390/en14123489

APPENDIX

APPENDIX A: MATLAB Script and Motor Drive Schematics for Training the Artificial Neural Network

Validation Ratios and Hidden Layer Configurations for ANN Training:

```
num_runs = 100;
train_ratios = [70];
val_ratios = [0, 5, 10, 15, 20, 25, 30];
hiddenLayerSizes = {[10], [20], [10, 10]};
```

Dynamic Partitioning of Dataset into Training, Validation, and Testing Sets:

```
for val_idx = 1:length(val_ratios)
val_ratio = val_ratios(val_idx);
test_ratio = 100 - train_ratios - val_ratio;
disp(['Train Ratio: ', num2str(train_ratios), '% | Validation Ratio: ',
num2str(val_ratio), '% | Test Ratio: ', num2str(test_ratio), '%']);
```

Iterative Configuration of Hidden Layer Sizes for ANN Architecture:

```
for hidden_idx = 1:length(hiddenLayerSizes)
hiddenLayerSize = cell2mat(hiddenLayerSizes(hidden_idx));
disp(['Hidden Layer Size: ', num2str(hiddenLayerSize)]);
```

Neural Network Training:

```
for run = 1:num_runs
input_neurons = Iregular_Wave_1331(:, 1:3)';
output_neurons = Iregular_Wave_1331(:, 4)';
net = feedforwardnet(hiddenLayerSize, 'trainlm');
net.divideParam.trainRatio = train_ratios / 100;
net.divideParam.valRatio = val_ratio / 100;
net.divideParam.testRatio = test_ratio / 100;
net.trainParam.showWindow = false;
[net, tr] = train(net, input_neurons, output_neurons);
net_filename = sprintf('network_train%d_val%d_hidden%s_run%d.mat',
train_ratios, val_ratio, strrep(num2str
(hiddenLayerSize), ' ', '_'), run);
save(fullfile(output_folder, net_filename), 'net');
```

Power Outputs Are Calculated with Using a Self-Controlled Synchronous 200 HP Motor Drive:

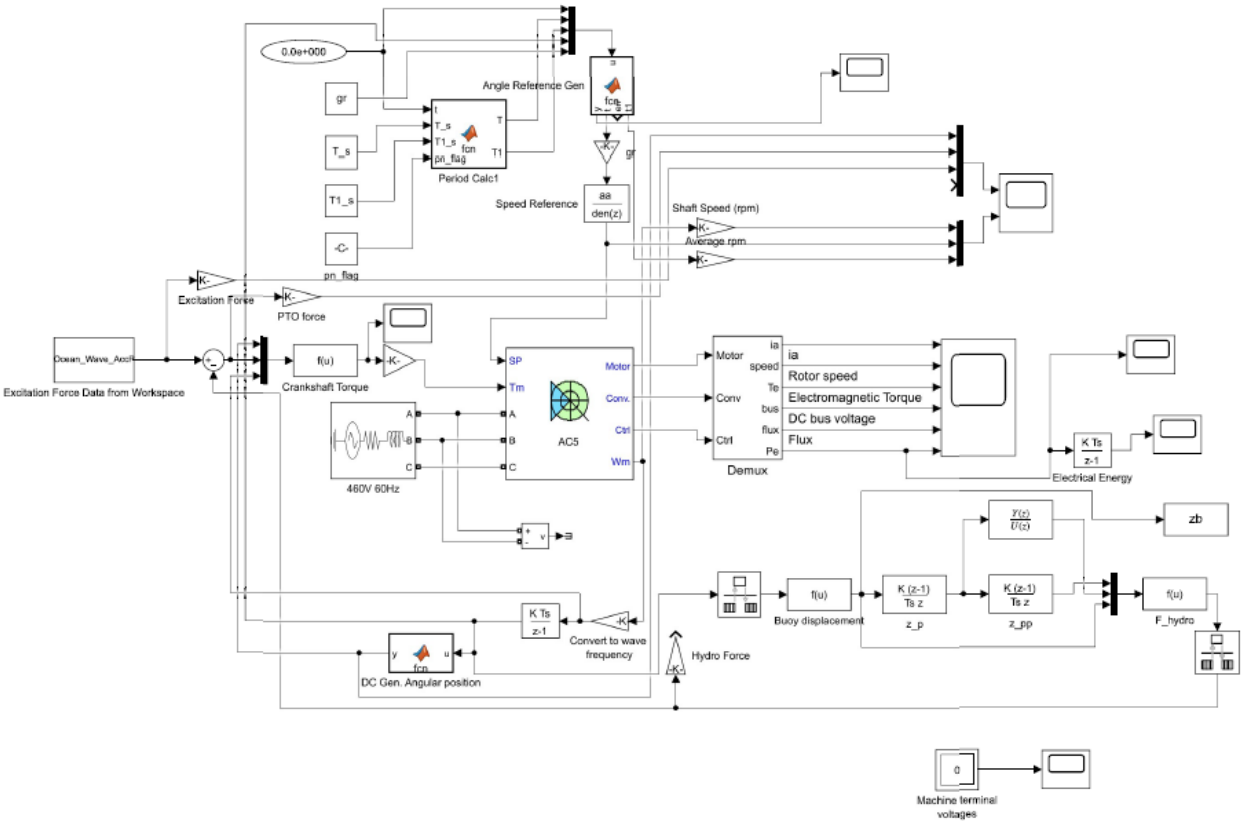

Figure A.1: Self-Controlled Synchronous 200 HP Motor Drive

Matlab Script to Calculate Mechanical Power Outputs using JONSWAP Model:

```
Ts=20e-6; % Sampling time
Td=1e-3; % Discrete Sampling time
%%% setting 1 %%%
gr=110;    % Gear ratio
%======================
aa=20e-6/(.5+20e-6);
%Slider-Crank initialization
global r                    % Radius of crank. used again in the rk4sys_step
function and slider crank function.
global l                    % Length of rod, used again in the slider crank
function.
global dr_dsb                    % (Used to be r+A) Distance between the
lowest edge of the crank and the reference water surface
r=.5;                    % Radius of crank. used again in the rk4sys_step
function and slider crank function.
l=1;                     % Length of rod, used again in the slider crank
function.
lambda=r/l;              % used again in the slider crank function.
B=0.01;                  % Viscous friction, used again in the slider crank
function.
```

```
J=10;                   % inertia of flywheel, used again in the slider crank
function.
dr_dsb=l;                   % (Used to be r+A) Distance between the lowest
edge of the crank and the reference water surface
mcrp=10;                % Total of mass of piston (or slider) and connecting
rod respectively.
% Hydrodynamics initialization (frequency domain)
delta_omega=0.01;
omega=0.5:delta_omega:1.4;
N=length(omega);
fn=omega/2/pi;% frequencies of the wave components
Hm0=1.1314; % significant wave height of the irregular wave. The same value
is used as that in "Effect of..."
Tp=6; % If this changes, int_S_star must be recalculated. Peak period of the
irregular wave. In "Effect of...", they used an average period of 6. We can
use our own to make the spectrum fit our need.
%%%=========================================%%%
fp=1/Tp;
g=9.81; % gravity acceleration
rho=1020;% water density
flag = 1; % 0 for Breschneider model and 1 for JONSWAP Model

switch flag
    case 0
      S=Hm0^2/4*(1.057*fp)^4*fn.^(-5).*exp(-5/4*(fp./fn).^4); %According to
WEC_Sim_User_Manual_v1.0.pdf
    case 1
% ====================  JONSWAP Model ================================%
        m0=sqrt(Hm0/4); % wave field variance. See "On control ...".
        %alpha=0.0081; % a given constant which is used in most references,
see "sea spectra revisited".
        gamma=6;% If this changes, int_S_star has to be recalculated. The
average of gamma is 3.3 (see "sea spectra revisited"). enhancement factor by
which the P_M peak energy is multiplied to get the peak energy value of the
spectrum.
        %Increasing gamma has the effect of reducing the spectral bandwidth,
        %thereby increasing periodicity of the wave field. See "On control
...".
        for i2=1:N
            if fn(i2)<=fp
                sigma=0.07;%if f<fp  sigma is the width factor of the
enhanced peak, see "sea spectra revisited". The numbers are given in "sea
spectra revisited".
            elseif fn(i2)>fp
                sigma=0.09;%if f>fp
            end
S(i2)=5*m0/fp*((fp/fn(i2))^5)*exp(-5/4*((fp/fn(i2))^4))*gamma^exp(-(fn(i2)-
fp)^2/(2*sigma^2*fp^2));
switch Tp
```

```
                case 6
                    int_S_star=11.9001+20.8213;
                case 7
                    int_S_star=22.0463+38.574;
                case 8
                    int_S_star=37.61+65.8056;
                case 9
                    int_S_star=60.244+105.408;
                case 10
                    int_S_star=91.8214+160.658;
            end
            alpha=Hm0^2/(int_S_star*16); %int_S_star should be changed when
Tp or gamma changes.
            GAMMA=exp(-((fn(i2)/fp-1)/(sqrt(2)*sigma))^2);
            S(i2)=alpha*g^2/(2*pi)^4*fn(i2)^(-5)*exp(-
5/4*(fp/fn(i2))^4)*gamma^GAMMA;
        end
end
Start_Time=0;              % time start
End_Time=500;              % final time
Interval=0.01;             % sampling time interval
t=Start_Time:Interval:End_Time;
M=length(t);

%%% setting 2 %%%
a=5; % buoy radius
%======================
c=rho*g*pi*a^2; % a coefficient that is used later
%%% setting 3 %%%
A=sqrt(2*S*delta_omega/2/pi); % calculate amplitude for each wave component
rng(0);
Phase=2*pi*rand(1,N); % randomly generate the initial phase of each wave
component
Ka=[0 0.05 0.1 0.2 0.3 0.4 0.5 0.6 0.7 0.8 0.9 1.0 1.2 1.4 1.6 1.8 2.0 2.5
3.0 4.0 5.0 6.0 7.0 8.0 9.0 10.0]';
Amass=[0.8310 0.8764 0.8627 0.7938 0.7157 0.6452 0.5861 0.5381 0.4999 0.4698
0.4464 0.4284 0.4047 0.3924 0.3871 0.3864 0.3884 0.3988 0.4111 0.4322 0.4471
0.4574 0.4647 0.4700 0.4740 0.4771]';
Damping=[0 0.1036 0.1816 0.2793 0.3254 0.3410 0.3391 0.3271 0.3098 0.2899
0.2691 0.2484 0.2096 0.1756 0.1469 0.1229 0.1031 0.0674 0.0452 0.0219 0.0116
0.0066 0.0040 0.0026 0.0017 0.0012]';
len=length(Ka);
kappa=zeros(1,len);
imkap=zeros(1,len);
rekap=zeros(1,len);
mm=rho*(2*pi/3)*a^3;
Sb=rho*g*pi*a^2;%785890;
kappa(1)=1;
imkap(1)= 2*Damping(1)*Ka(1)/3;
```

```
rekap(1)= sqrt(kappa(1)^2-imkap(1)^2);
for j=2:len
    kappa(j)= sqrt(4*Damping(j)/(3*pi*Ka(j)));
    imkap(j)= 2*Damping(j)*Ka(j)/3;
    rekap(j)= sqrt(kappa(j)^2-imkap(j)^2);
end

Kaq=omega.^2/g*a;
kappa_im=zeros(1,N);
kappa_re=zeros(1,N);
kappa_angle=zeros(1,N);
kappa_abs=zeros(1,N);
for i1=1:N
    kappa_abs(i1)=interp1(Ka,kappa,Kaq(i1),'pchip');
    kappa_im(i1)=interp1(Ka,imkap,Kaq(i1),'pchip');
    kappa_re(i1)=interp1(Ka,rekap,Kaq(i1),'pchip');
    kappa_angle(i1)=atan(kappa_im(i1)/kappa_re(i1));
end
for i=1:N
    eta{i}=@(t)A(i)*sin(omega(i)*t+Phase(i)+kappa_angle(i));
    Fe_components{i}=@(t)c*kappa_abs(i)*eta{i}(t);
    Fe=@(t)Fe(t)+Fe_components{i}(t);
    eta_total=@(t)eta_total(t)+eta{i}(t);
end
```

APPENDIX B: MATLAB Script for Finding Optimal Time Shift Using Binary Search Algorithm

```
Wave_Height = [];              % Significant wave height (Hm0) in meters
Peak_Period = [];                    % Peak period (Tp) in seconds
Time_Shift = 0:0.5:0.30;             % Time shift values to evaluate

max_Power_Output = [];               % Matrix to store results

% Loop through each wave height value
for i = 1:length(Wave_Height)
    Hm0 = Wave_Height(i);

    % Loop through each peak period value
    for j = 1:length(Peak_Period)
        Tp = Peak_Period(j);

        % Apply binary search to find optimal time shift
        left = 1;
        right = length(Time_Shift);

        while left <= right
            mid1 = floor(left + (right - left) / 3);
            mid2 = floor(right - (right - left) / 3);

            Hm0_mid1 = Time_Shift(mid1);
            Hm0_mid2 = Time_Shift(mid2);

            % Predict power output for both midpoints
            ans_mid1 = net([Hm0; Tp; Hm0_mid1]);
            ans_mid2 = net([Hm0; Tp; Hm0_mid2]);

            % Adjust search range based on comparison
            if ans_mid1 < ans_mid2
                left = mid1 + 1;
            else
                right = mid2 - 1;
            end
        end

        % Store the best time shift and corresponding power output
        bestHm0 = Time_Shift(left);
        maxPower = net([Hm0; Tp; bestHm0]);
        max_Power_Output(end+1, :) = [Hm0, Tp, bestHm0, maxPower];
    end
end
```

APPENDIX C: ANN Configuration Performance

ANN Configuration Performance Matrix for Regular Waves

all_results_matrix.csv

	A	B	C	D	E	F
				allresultsmatrix		
	Train_Ratio	Val_Ratio	Hidden_Layer_Size_1	Hidden_Layer_Size_2	Minimum_Error_Rate	Best_Run_Number
	Number	Number	Number	Number	Number	Number
1	Train_Ratio	Val_Ratio	Hidden_Layer_Size_1	Hidden_Layer_Size_2	Minimum_Error_Rate	Best_Run_Number
2	70	0	10		1.18281237455207	4
3	70	0	20		1.02418541887133	7
4	70	0	10	10	0.803874300097329	7
5	70	5	10		1.5078678050303	8
6	70	5	20		1.18970686137798	4
7	70	5	10	10	1.01442187098644	4
8	70	10	10		1.39804705068859	9
9	70	10	20		1.11382864613561	5
10	70	10	10	10	0.974906295491596	6
11	70	15	10		1.20049100727706	7
12	70	15	20		1.01646224245227	6
13	70	15	10	10	0.957683938202598	2
14	70	20	10		1.61489991235589	5
15	70	20	20		1.15607775733102	5
16	70	20	10	10	0.824654432069564	3
17	70	25	10		1.34048721323435	4
18	70	25	20		0.976331139738763	3
19	70	25	10	10	0.95552982659444	6
20	70	30	10		1.52259259064937	5
21	70	30	20		1.16763196228415	1
22	70	30	10	10	0.94161909696087	6

Figure A.2: ANN Configuration Performance Matrix for Regular Waves

ANN Configuration Performance Matrix for Irregular Waves

	A	B	C	D	E	F	G	H
	Train_Ratio	**Val_Ratio**	**Test_Ratio**	**Hidden_Layer_Size_1**	**Hidden_Layer_Size_2**	**Num_Runs**	**Min_Error_Rate**	**Std_Dev**
	Number	Number	Number	Number	Number	Number	Number	Number
1	Train_Ratio	Val_Ratio	Test_Ratio	Hidden_Layer_Size_1	Hidden_Layer_Size_2	Num_Runs	Min_Error_Rate	Std_Dev
2	70	0	30	10		100	1.408815129	7.761196828
3	70	0	30	20		100	0.992963224	21.55946498
4	70	0	30	10	10	100	0.464684557	5.174958082
5	70	5	25	10		100	1.804680647	0.717000241
6	70	5	25	20		100	1.067390001	0.50617817
7	70	5	25	10	10	100	0.684693593	5.19865943
8	70	10	20	10		100	1.712092405	0.500572502
9	70	10	20	20		100	1.056876302	0.686291784
10	70	10	20	10	10	100	0.630343386	5.148291162
11	70	15	15	10		100	1.606726454	0.584951946
12	70	15	15	20		100	1.080905849	1.189625423
13	70	15	15	10	10	100	0.591679622	5.130921377
14	70	20	10	10		100	1.609457104	0.395322799
15	70	20	10	20		100	0.995173488	1.653650368
16	70	20	10	10	10	100	0.604834078	5.219030061
17	70	25	5	10		100	1.606726454	0.521703415
18	70	25	5	20		100	1.145566081	0.672972162
19	70	25	5	10	10	100	0.591679622	5.135356371
20	70	30	0	10		100	1.613489173	0.799551432
21	70	30	0	20		100	0.993328217	1.328898408
22	70	30	0	10	10	100	0.549432597	5.164315008

Figure A.3: ANN Configuration Performance Matrix for Irregular Waves

APPENDIX D: Neural Network Weights and Biases

Neural Network Weights and Biases for Regular Waves:

Table A.1: Weights from Input Layer to First Hidden Layer

-0.3690	0.0686	0.4797
-0.1692	-0.1214	-0.6474
0.6671	0.9741	0.0661
-1.0120	-1.3879	-0.1654
-0.1633	0.6309	-1.2089
-0.3597	-0.0741	0.2595
0.0133	-0.1334	-0.6531
-3.1397	-17.0616	-11.5478
1.1569	-5.8678	0.1671
-0.9243	3.9399	0.0749

Table A.2: Weights from Hidden Layer 1 to Hidden Layer 2

1.0684	0.6091	2.0255	-0.4907	1.9070	-1.3625	-0.1048	0.2121	1.6246	2.4146
1.3845	0.0764	-6.0312	-3.5639	2.1394	-1.2406	0.0097	0.1258	-0.8890	-0.9651
-1.8584	-0.9807	-0.4284	-0.5531	-0.2915	2.4621	0.9110	-0.0714	-0.8638	-1.3044
4.7756	0.2079	3.7307	1.9604	3.1842	-0.7412	-2.1837	-0.2448	-5.1852	-7.5518
1.6308	0.4971	0.0255	-1.3872	2.6785	-2.1187	-0.0161	0.2252	1.5020	2.3784
-1.8226	-1.5418	-0.0647	2.3947	-0.1865	-1.8632	3.5960	-0.5764	4.8988	4.4826
2.0760	1.8647	6.4105	3.6980	0.1483	-2.8279	-0.9440	0.3248	2.3593	2.7195
-3.9780	0.0292	-0.0205	0.0352	0.2679	4.3259	-0.1425	-0.0325	0.1423	0.2225
-0.4654	-0.6446	-3.7501	-2.3362	0.7767	0.9396	0.6278	0.0178	-0.9216	-1.2535
2.4622	-0.2273	-5.3824	-2.9118	-1.6627	-4.2811	1.5980	0.6138	3.0574	4.9744

Table A.3: Weights from Second Hidden Layer to Output Layer:

-3.4089	-5.3035	-9.0289	0.1833	4.1085	-0.1865	-0.7633	-3.6063	15.0251	-0.6570

Table A.4: Hidden Bias 1

1.36222400675411
-0.0898996687761619
-1.03988188844596
0.993003653065467
2.75766642385483
0.964796536775516
0.270550175666627
15.8160919839856
5.62674023463567
-4.23759238659955

Table A.5: Hidden Bias 2

0.986048071846016
-5.00505864707273
-1.37171357878106
-7.34917540353912
-0.454913274165499
4.07573684263369
1.54149540543917
-0.727040949336687
-3.68138044354589
3.53460868468031

Table A.6: Output Bias 1

0.0857555516361454

Neural Network Weights and Biases for Irregular Waves:

Table A.7: Weights from Input Layer to First Hidden Layer

-1.8858	8.4391	-0.5553
-0.3200	-2.6661	-0.3623
0.0228	-0.1528	-0.3437
0.2849	-1.1397	-0.0167
0.4980	-0.2754	-0.2978
0.2330	-2.8373	0.0571
0.1610	-0.6403	0.4261
-0.0858	3.8806	0.1416
-0.6206	0.1064	0.2276
0.5906	-0.9957	-0.2321

Table A.8: Weights from Hidden Layer 1 to Hidden Layer 2

-0.0303	0.4205	-0.5900	1.9575	-1.1710	0.0274	-1.6362	0.0091	-1.4117	1.3960
-2.4568	-8.6251	-1.8911	3.2583	8.2206	-0.6240	-1.1319	2.6111	4.0365	11.9545
-0.0616	-2.0628	1.2670	2.2781	-4.1318	0.2813	-0.8582	0.8047	-4.2538	-1.2231
-0.1766	-0.6375	-2.0937	0.3105	2.9754	-1.4871	2.5945	1.0563	1.8840	0.8799
0.0083	-0.1558	-1.0201	2.5596	0.6293	-0.0321	-1.1276	0.4904	-0.1121	0.6670
-0.1469	-2.0711	1.2284	-0.1210	-3.1729	0.3794	-0.6479	0.6916	-3.6812	-1.6234
11.9378	-7.2312	-1.9798	6.0786	-0.3943	-2.1662	0.3336	1.3204	0.8004	2.3023
-0.0038	1.1792	-3.3597	-1.4416	2.7670	-0.0386	0.3017	0.1300	0.9809	0.1680
0.0114	-0.4583	-0.5712	2.1387	-3.3098	-0.5233	-2.6060	0.9535	-1.9970	3.2184
0.0365	0.0360	0.1452	-2.0277	0.7983	-0.0904	1.3352	-0.2807	1.1964	-0.7268

Table A.9: Weights from Second Hidden Layer to Output Layer:

7.4130	-0.0127	-3.3203	-0.8905	6.4143	3.2420	0.2391	-0.8611	7.2091	10.1539

Table A.10: Hidden Bias 1

4.68899360515219
2.63191653427654
-0.525554228470262
-2.25183982736615
0.151805650309228
0.424371036396322
-1.44506021501034
2.42984355980528
-0.399122109459879
0.952939225417872

Table A.11: Hidden Bias 2

-2.48924780844310
-2.29009214694376
3.97459079381221
0.384939358555616
0.210603548522940
2.10325306842873
-2.15971658940740
-4.38842148781186
1.08921283342695
0.736513755396958

Table A.12: Output Bias 1

-6.27883364210112

APPENDIX E: Overall RM3 WEC system

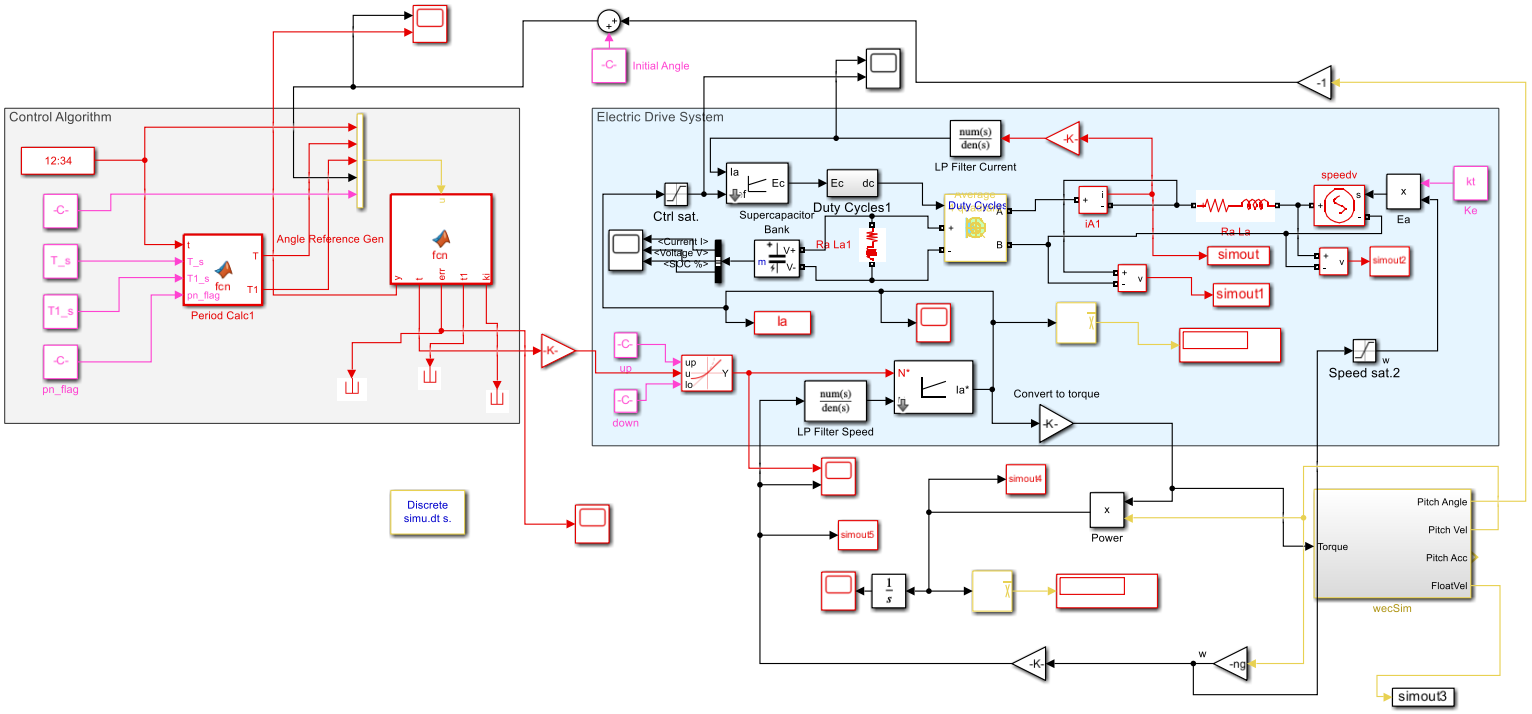

Figure A.4: Overall RM3 WEC system

APPENDIX F: Linemodifier Script

```
tic
clear
Value1 = input('Enter the value for wave height (H): ');
Value2 = input('Enter the value for wave period (T): ');
Value3 = input('Enter the value for Time Shift (TS): ');

%If there is no time shift needed put “0”.

filename = 'wecSimInputFile.m';

% Read the file into a cell array
fileContent = {};
fid = fopen(filename, 'r');
tline = fgetl(fid);
while ischar(tline)
    fileContent{end+1} = tline;
    tline = fgetl(fid);
end
fclose(fid);

scale=2; %Wave Energy Converter Scaler (Full for 1, Half for 2, 1/3 for 3)

% Lines 85 and 86 needs to be change in wecSimInputFile with the desired Wave
%height and Wave period in order to calculate Mechanical and Electrical Power
%Output
% Modify lines 85 and 86 with new wave height and period
fileContent{85} = sprintf('waves.H = scale*%g/Ls;', Value1);
fileContent{86} = sprintf('waves.T = sqrt(scale)*%g/Tsc;', Value2);

% Write the modified content back to the file
fid = fopen(filename, 'w');
for i = 1:length(fileContent)
    fprintf(fid, '%s\n', fileContent{i});
end
fclose(fid);

disp('Successfully updated waves.H and waves.T in wecSimInputFile.m');

wecSim;

% Create a folder named HValue1_TValue2
folder_name = sprintf('H%g_T%g', Value1, Value2);

if ~exist(folder_name, 'dir')
    mkdir(folder_name);
    disp(['Folder created: ', folder_name]);
else
    disp(['Folder already exists: ', folder_name]);
end

% Save Body_out1 in both the current directory and the new folder
if exist('body1_out', 'var')
    % Save in the current directory
    filename_save_current = sprintf('ex_1_H%g_T%g.mat', Value1, Value2);
```

```
    save(filename_save_current, 'body1_out');
    disp(['Body_out1 has been saved as ', filename_save_current, ' in the
current directory.']);

    % Save in the new folder
    save(fullfile(folder_name, 'body1_out.mat'), 'body1_out');
    disp(['Body_out1 has been saved in folder ', folder_name]);
else
    disp('Body_out1 does not exist in the workspace. Make sure to run the
simulation first.');
end

% Now rewrite line 1 of Wave_Analysis_WEC_Sim.m
wave_analysis_filename = 'Wave_Analysis_WEC_Sim.m';

% Read the file into a cell array
fileContent = {};
fid = fopen(wave_analysis_filename, 'r');
tline = fgetl(fid);
while ischar(tline)
    fileContent{end+1} = tline;
    tline = fgetl(fid);
end
fclose(fid);

% Create the new line to load the correct .mat file
new_line = sprintf('load ex_1_H%g_T%g.mat', Value1, Value2);
new_line2 = sprintf('T1_s=T1_s+(%g);', Value3);

% Modify line 1
fileContent{1} = new_line;
fileContent{28} = new_line2;
% Write the modified content back to the file
fid = fopen(wave_analysis_filename, 'w');
for i = 1:length(fileContent)
    fprintf(fid, '%s\n', fileContent{i});
end
fclose(fid);

disp('Successfully updated line 1 in Wave_Analysis_WEC_Sim.m');
wecSim;

% Save other variables (simout, simout1, simout2, simout3, simout4, simout5)
%into the folder
variables_to_save = {'simout', 'simout1', 'simout2', 'simout3', 'simout4',
'simout5','body1_out'};

for i = 1:length(variables_to_save)
    if exist(variables_to_save{i}, 'var')
        save(fullfile(folder_name, [variables_to_save{i}, '.mat']),
variables_to_save{i});
        disp([variables_to_save{i}, ' has been saved in folder ',
folder_name]);
    else
        disp([variables_to_save{i}, ' does not exist in the workspace.']);
    end
end
```

```
a=cumsum(-simout.data.*simout1.data*5e-4);a(end) % Generator Terminal Power
a=cumsum(-simout.data.*simout2.data*5e-4);a(end) % Back EMF Terminal Power
a=cumsum(simout4.data*5e-4);a(end) % Mechanical Power
toc

format bank
a=cumsum(simout4.data*5e-4);a(end)
mech_en=a;
tt=find(abs(simout4.time-300)<5e-4);
P_Ave=(mech_en(end)-mech_en(end-tt(1)))/simout4.time(tt(1));
Average_Mechanical_Power=P_Ave*7.5^3.5

elec_pw=-simout.data.*simout1.data;
elec_en=cumsum(elec_pw*5e-4);elec_en(end)
PE_Ave=(elec_en(end)-elec_en(end-tt(1)))/simout4.time(tt(1));

%To calculate the electrical power multiply scaled WEC (For full scale
%15^3.5, Half scale 7.5^3.5, 1/3 scale 5^3.5) with PE_average
Average_Elec_Power=PE_Ave*7.5^3.5
```

APPENDIX G: Device Cost Calculator for System Advisor Model (SAM)

```
structural_assembly_full = 236938161; % Full-scale structural assembly cost

pto_full = 52489652; % Power take-off system cost for 286 kW

mooring_full = 93918662; % Mooring cost for 360 kW

scale = input('Enter the scale: ');

power_rating = input('Enter the power rating in kW: ');

arraysize = input('Enter the arraysize: ');

costscale = input('Cost scaling exponent: ');

structural_assembly_cost = ((structural_assembly_full/100)*arraysize) /
scale^costscale; %scale^3

pto_cost = ((pto_full * power_rating/100)*arraysize) / 286;

mooring_cost = ((mooring_full * power_rating/100)*arraysize) / 360;

total_cost = structural_assembly_cost + pto_cost + mooring_cost;

fprintf('Structural Assembly Cost: $%.2f\n', structural_assembly_cost);

fprintf('Power Take-Off System Cost: $%.2f\n', pto_cost);

fprintf('Mooring Foundation and Substructure Cost: $%.2f\n', mooring_cost);

fprintf('Total Estimated Cost: $%.2f\n', total_cost);
```